Atrial Natriuretic Peptide Orchestrates a Coordinated Physiological Response to Fuel Non-shivering Thermogenesis

Deborah Carper, Marine Coué, Emmani B.M. Nascimento, Valentin Barquissau, Damien Lagarde, Carine Pestourie, Claire Laurens, Justine Vily Petit, Maud Soty, Laurent Monbrun, et al.

Cell Reports

Article

Atrial Natriuretic Peptide Orchestrates a Coordinated Physiological Response to Fuel Non-shivering Thermogenesis

Graphical Abstract

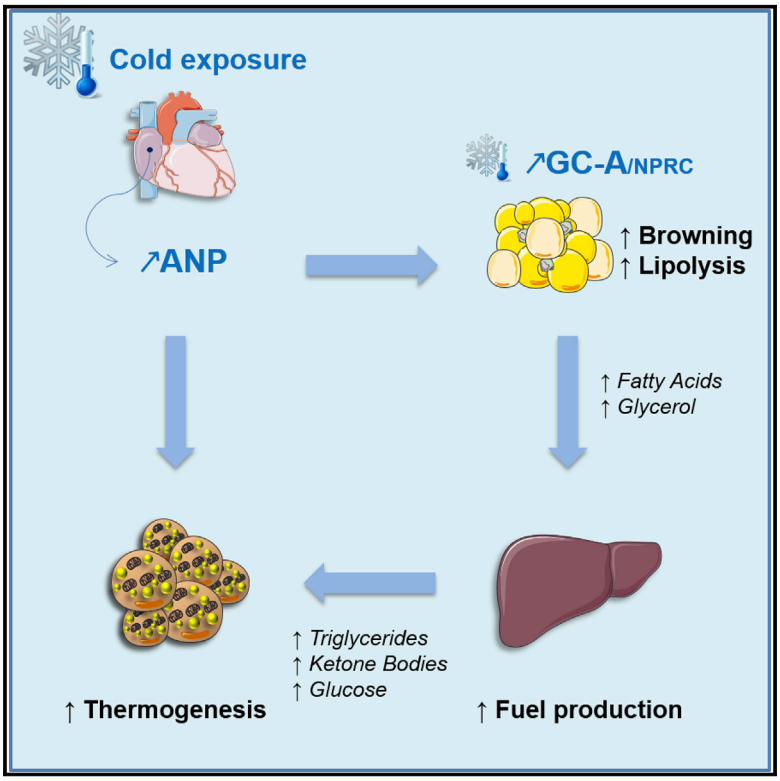

Highlights

- Cold exposure induces the ANP receptor GCA in BAT and WAT
- ANP substantially contributes to BAT thermogenesis during cold exposure
- WAT lipolysis and liver substrate production depend on ANP during cold exposure
- ANP increases thermogenesis in human BAT and WAT adipocytes

Authors

Deborah Carper, Marine Coué, Emmani B.M. Nascimento, ..., Dominique Langin, Patrick Schrauwen, Cedric Moro

Correspondence

cedric.moro@inserm.fr

In Brief

The classical view is that brown adipose tissue (BAT) is mainly activated by the sympathetic nervous system. Carper et al. here demonstrate that the cardiac hormone atrial natriuretic peptide is released upon cold exposure and required to activate BAT thermogenesis and white fat browning in mice and humans.

Carper et al., 2020, Cell Reports *32*, 108075
August 25, 2020
https://doi.org/10.1016/j.celrep.2020.108075

CellPress

Cell Reports

CellPress
OPEN ACCESS

Article

Atrial Natriuretic Peptide Orchestrates a Coordinated Physiological Response to Fuel Non-shivering Thermogenesis

Deborah Carper,[1,2] Marine Coué,[1,2] Emmani B.M. Nascimento,[3] Valentin Barquissau,[1,2] Damien Lagarde,[2,4] Carine Pestourie,[5] Claire Laurens,[1,2] Justine Vily Petit,[6] Maud Soty,[6] Laurent Monbrun,[1,2] Marie-Adeline Marques,[1,2] Yannick Jeanson,[4] Yannis Sainte-Marie,[1,2] Aline Mairal,[1,2] Sébastien Déjean,[7] Geneviève Tavernier,[1,2] Nathalie Viguerie,[1,2] Virginie Bourlier,[1,2] Frank Lezoualc'h,[1,2] Audrey Carrière,[2,4] Wim H.M. Saris,[3] Arne Astrup,[8] Louis Casteilla,[2,4] Gilles Mithieux,[6] Wouter van Marken Lichtenbelt,[3] Dominique Langin,[1,2,9] Patrick Schrauwen,[3] and Cedric Moro[1,2,10,*]

[1]INSERM, UMR1048, Institute of Metabolic and Cardiovascular Diseases, Toulouse, France
[2]University of Toulouse, UPS, Toulouse, France
[3]NUTRIM School for Nutrition and Translational Research in Metabolism, Maastricht University Medical Center, Maastricht, the Netherlands
[4]INSERM, UMR1031, STROMA Lab, CNRS, EFS, ENVT, INSERM U1031, ERL 5311, Toulouse, France
[5]CREFRE, University of Toulouse, INSERM UMS006, UPS, ENVT, Team Non Invasive Exploration, Toulouse, France
[6]INSERM U1213, Nutrition, Diabète et Cerveau, Lyon, France
[7]Toulouse Mathematics Institute, UMR 5219, CNRS, University of Toulouse, Toulouse, France
[8]Department of Nutrition, Exercise and Sports, Faculty of Sciences, University of Copenhagen, Copenhagen, Denmark
[9]Toulouse University Hospitals, Department of Clinical Biochemistry, Toulouse, France
[10]Lead Contact
*Correspondence: cedric.moro@inserm.fr
https://doi.org/10.1016/j.celrep.2020.108075

SUMMARY

Atrial natriuretic peptide (ANP) is a cardiac hormone controlling blood volume and pressure in mammals. It is still unclear whether ANP controls cold-induced thermogenesis *in vivo*. Here, we show that acute cold exposure induces cardiac ANP secretion in mice and humans. Genetic inactivation of ANP promotes cold intolerance and suppresses half of cold-induced brown adipose tissue (BAT) activation in mice. While white adipocytes are resistant to ANP-mediated lipolysis at thermoneutral temperature in mice, cold exposure renders white adipocytes fully responsive to ANP to activate lipolysis and a thermogenic program, a physiological response that is dramatically suppressed in ANP null mice. ANP deficiency also blunts liver triglycerides and glycogen metabolism, thus impairing fuel availability for BAT thermogenesis. ANP directly increases mitochondrial uncoupling and thermogenic gene expression in human white and brown adipocytes. Together, these results indicate that ANP is a major physiological trigger of BAT thermogenesis upon cold exposure in mammals.

INTRODUCTION

Warm-blooded animals have acquired the ability to maintain a constant core body temperature in fluctuating temperature environments through an adaptive physiological process called thermogenesis. Brown adipose tissue (BAT) is considered the major site of non-shivering thermogenesis and heat production, which allows rodents to maintain euthermia at temperatures below thermoneutrality (Nedergaard and Cannon, 2010).

Thermogenic fat cells include brown and beige adipocytes, cells that play a critical role in defending against hypothermia, obesity, and diabetes through dissipating chemical energy as heat in part through mitochondrial uncoupling protein 1 (UCP1) (Kajimura et al., 2015). Thermogenic genes can be readily induced in brown and beige adipocytes within white adipose tissue (WAT) in response to cold exposure (Cannon and Nedergaard, 2004; Harms and Seale, 2013; Wu et al., 2012). When activated, thermogenic adipocytes consume a large amount of circulating triglycerides, glucose, and non-esterified fatty acid (NEFA) (Heine et al., 2018). The long-standing prevailing view is that cold sensation is primarily transmitted through the sympathetic nervous system. BAT and WAT are innervated by sympathetic fibers (Jiang et al., 2017), which, upon cold exposure, release norepinephrine to acutely activate thermogenesis and lipolysis. Norepinephrine activates β_3-adrenergic receptors and cyclic AMP (cAMP)-dependent protein kinase (PKA), which elicit a signaling cascade via p38 mitogen-activated protein kinase (MAPK) and peroxisome proliferator-activated receptor γ (PPARγ) co-activator 1α (PGC1α) to increase the transcription of UCP1 and thermogenic genes in brown adipocytes (Cao et al., 2004). In WAT, β_3-adrenergic signaling activates adipocyte lipolysis through adipose triglyceride lipase (ATGL) and hormone-sensitive lipase (HSL). WAT lipolysis is essential to provide fatty acid (FA) fuels in the fasting state to sustain high respiration rates in BAT (Schreiber et al., 2017; Shin et al., 2017).

Yet, recent studies indicate that β_3-adrenergic receptor is dispensable in brown and beige adipocyte for cold-induced transcriptional activation of thermogenic genes in mice (de Jong et al., 2017). Studies in mice lacking all three β-adrenergic receptors (so-called β-less mice) inferred the existence of non-adrenergic signaling pathways contributing to brown/beige adipocyte recruitment and activation (Bachman et al., 2002; Jiang et al., 2017). Studies over the past few years identified a variety of circulating factors and hormones that may control beige adipocyte development of which cardiac natriuretic peptides (NPs) are of particular interest. NPs control blood volume and pressure in mammals (Kuhn, 2016) and were shown to be potent lipolytic hormones in human WAT (hWAT) (Moro et al., 2004; Sengenès et al., 2000). Moreover, NPs induce the transcription of *PGC1α* and *UCP1* via cGMP-dependent protein kinase (PKG) *in vitro* in human adipocytes (Bordicchia et al., 2012). Chronic B-type NP (BNP) infusion in mice induces *Pgc1α* and *Ucp1* in BAT and inguinal WAT (iWAT) (Bordicchia et al., 2012). However, although NPs induce a transcriptional thermogenic program in adipocytes, it is unclear if they are necessary and required for physiological activation of brown/beige adipocytes during acute cold exposure. Here, we show that cardiac atrial NP (ANP) is a critical physiological endocrine regulator of non-shivering thermogenesis in mammals.

RESULTS

ANP Is Required for Non-shivering Thermogenesis during Acute Cold Exposure

[^{18}F]Fluorodeoxyglucose positron emission tomography-computed tomography (^{18}F-FDG PET/CT) imaging indicate that acute cold exposure at 4°C for 5 h induces the recruitment of several BAT depots in the neck (anterior cervical) and clavicular areas (clavicular, axillary, supraspinal, interscapular, infrascapular, anterior subcutaneous, ventral spinal, and perirenal) in wild-type mice (Figures 1A and S1A). This is consistent with a recent study reporting similar recruitment of BAT depots in response to 7-day treatment with a β_3-adrenergic agonist (Zhang et al., 2018). BAT activation upon cold exposure was associated with a 3- to 4-fold increase of cardiac *Nppa* (ANP) expression (Figure 1B) and a 2-fold increase of plasma ANP (Figure 1C), while no change in cardiac *Nppb* (BNP) expression (Figure 1D) and plasma BNP (Figure 1E) was observed. Thus, this demonstrates that ANP rather than BNP behaves as a physiological endocrine ligand of guanylyl cyclase A (GCA) in response to cold stress. Cold exposure increases blood pressure and cardiac filling pressure, which are the main physiological stimuli of cardiac ANP secretion (Yuan et al., 2009).

To delineate the role of ANP in non-shivering thermogenesis, we next challenged ANP null mice (*Nppa*$^{-/-}$) at 4°C. *Nppa*$^{-/-}$ mice had no detectable cardiac *Nppa* expression (Figure S1B) and no functional compensation by either cardiac *Nppb* expression (Figure S1C) or plasma BNP (Figure S1D) upon cold exposure. ANP deficiency was associated with the development of cardiac hypertrophy, as shown by the increased heart weight to body weight ratio (Figure S1E) and left ventricular mass (Figure S1F). Since an intact cardiac function is required for functional non-shivering thermogenesis upon acute cold exposure (Schreiber et al., 2017), we show here that cardiac hypertrophy in *Nppa*$^{-/-}$ mice does not alter systolic function, since left ventricular ejection fraction remains comparable to wild-type littermates (*Nppa*$^{+/+}$) (Figure S1G). *Nppa*$^{-/-}$ mice had normal rectal temperature at room temperature (RT; 21°C) (Figure 1F) and at thermoneutrality (30°C) (Figure 1H) compared with their wild-type littermates but became cold intolerant upon acute cold exposure (Figure 1G). Since BAT is the main site of non-shivering thermogenesis, we measured BAT activity and recruitment by ^{18}F-FDG PET/CT in *Nppa*$^{+/+}$ and *Nppa*$^{-/-}$ mice at RT and 4°C (Figure 1H). Acute cold remarkably increased BAT ^{18}F-FDG uptake and metabolic volume, while cold-induced BAT ^{18}F-FDG uptake (5.9 versus 12.7 fold, $p < 0.01$) (Figure 1I) and ^{18}F-FDG metabolic volume (Figure 1J) (4.8- versus 9.7-fold, $p < 0.05$) were both severely blunted in *Nppa*$^{-/-}$ versus *Nppa*$^{+/+}$ mice. This effect may be ascribed to the lack of ANP, since the expression level of genes involved in ANP signaling such as *Gca*, NP clearance receptor (*Nprc*), and cGMP-dependent protein kinase (*Prkg1*) was comparable in BAT of *Nppa*$^{-/-}$ and *Nppa*$^{+/+}$ mice (Figure S1I). Fractional ^{18}F-FDG uptake by the hindlimb muscle quadriceps was reduced in *Nppa*$^{-/-}$ mice at 21°C and very low at 4°C (<1% of BAT) but remained unchanged between both genotypes (Figure 1K). Since β-adrenergic receptors (Bachman et al., 2002) (Figures S1J, S1K, and S1L) and adenosine receptors (Gnad et al., 2014) (Figures S1M and S1N) have been linked to BAT thermogenesis, we measured their gene expression levels and did not find significant changes between genotypes. Altogether, ANP deficiency severely blunts physiological BAT activation and recruitment.

ANP Deficiency Induces BAT Morphological and Molecular Changes

Histological analysis of BAT morphology revealed the presence and accumulation of multiple and large lipid droplets in *Nppa*$^{-/-}$ compared with *Nppa*$^{+/+}$ mice after cold exposure (Figure 2A). The BAT morphology of *Nppa*$^{-/-}$ mice at 4°C resembles the one observed at thermoneutral temperature (30°C) in both genotypes (Figure S2A), which is characteristic of a dysfunctional BAT. Since BAT is a highly vascularized tissue (Kajimura et al., 2015) and GCA activation can modulate angiogenesis in some vascular beds (Mallela et al., 2013), we next investigated BAT vascularization through lectin staining. No visual difference in BAT capillary density was observed between *Nppa*$^{-/-}$ and *Nppa*$^{+/+}$ (Figure S2B). Compared to what is observed after 4°C exposure, no visual difference in BAT morphology (Figure S2A) and expression levels of thermogenic genes (Figure S2C) were noted at RT between *Nppa*$^{-/-}$ and *Nppa*$^{+/+}$ mice. In contrast, cold-induced *Ucp1* (Figure 2B) and *Pgc1α* (Figure 2C) gene expression was severely blunted in *Nppa*$^{-/-}$ mice. We further confirmed a significant reduction of UCP1 protein content in interscapular BAT (iBAT) at 4°C in *Nppa*$^{-/-}$ mice (Figure 2D). Consistent with an impaired cold-induced BAT activation, we observed a blunted cold-mediated response of two canonical PPAR-target genes (Mandard et al., 2004; de la Rosa Rodriguez and Kersten, 2017), carnitine palmitoyl transferase-1B (*Cpt1b*) (Figure 2E) and perilipin 2 (*Plin2*) (Figure 2F), in *Nppa*$^{-/-}$ mice. Previous work has shown that PGC1α, once induced by acute cold, co-activates PPARγ, a crucial nuclear receptor

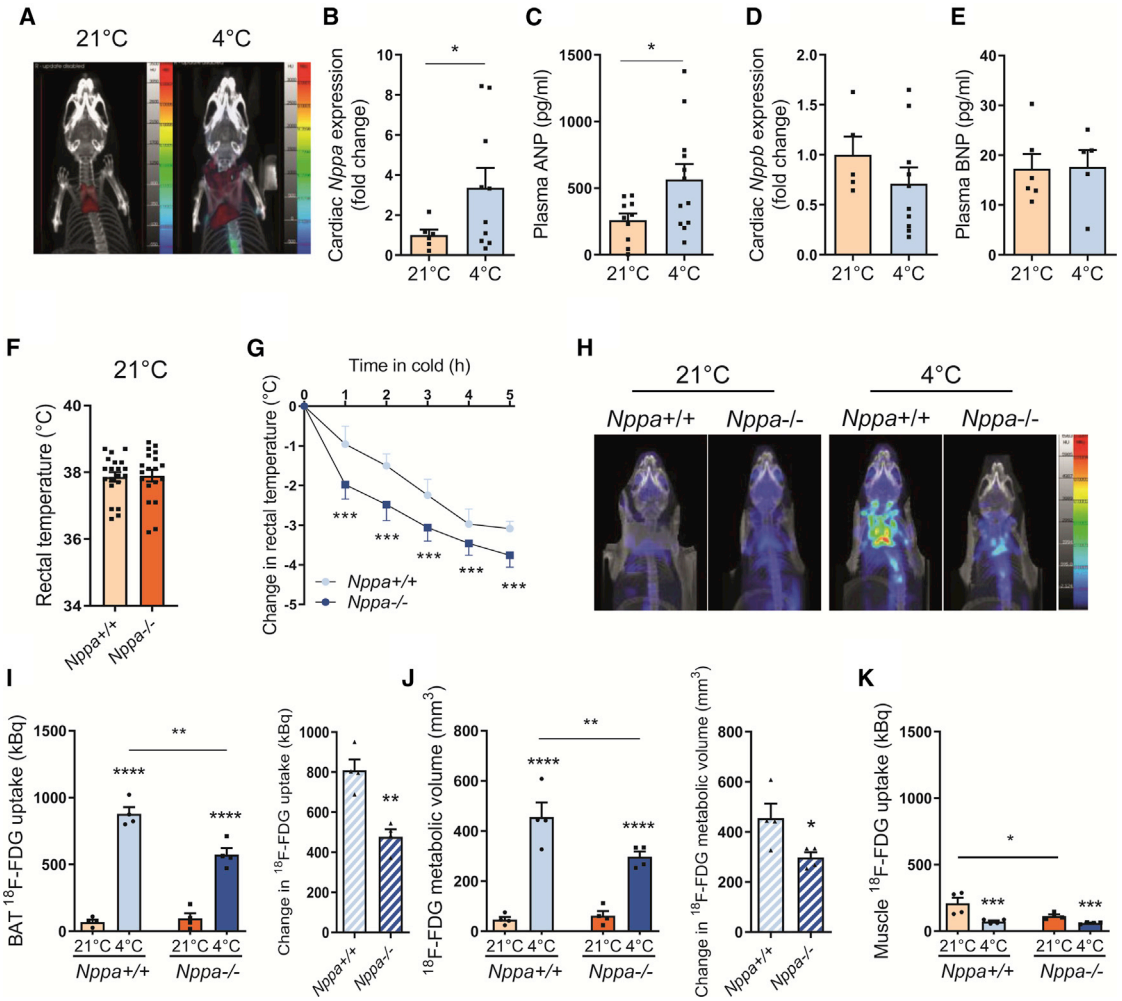

Figure 1. ANP Is Required for Non-shivering Thermogenesis during Acute Cold Exposure

(A) Representative ^{18}F-FDG PET/CT images of BAT recruitment around the neck in wild-type (WT) mice at room temperature (RT) (21°C) and exposed for 5 h to 4°C.

(B) Relative cardiac *Nppa* (ANP) expression in WT mice housed at RT (n = 6) and after acute cold exposure (5 h at 4°C) (n = 10).

(C) Plasma ANP levels in WT mice housed at RT (n = 10) and after acute cold exposure (n = 12).

(D) Relative cardiac *Nppb* (BNP) expression in WT mice housed at RT (n = 5) and after acute cold exposure (n = 10).

(E) Plasma BNP levels in WT mice housed at RT (n = 6) and after acute cold exposure (n = 5).

(F) Rectal temperature in *Nppa*$^{+/+}$ (n = 19) and *Nppa*$^{-/-}$ mice (n = 20) housed at RT.

(G) Change in rectal temperature from baseline in *Nppa*$^{+/+}$ (n = 7) and *Nppa*$^{-/-}$ (n = 5) mice during 5-h cold exposure.

(H) Representative ^{18}F-FDG PET/CT images of the neck/shoulder area indicating BAT activity in *Nppa*$^{+/+}$ and *Nppa*$^{-/-}$ mice at RT and during cold exposure.

(I) Quantitative scatterplot graph of BAT ^{18}F-FDG uptake and cold-induced BAT ^{18}F-FDG uptake of *Nppa*$^{+/+}$ and *Nppa*$^{-/-}$ mice at RT and during cold exposure (n = 4).

(J) Quantitative scatterplot graph of BAT ^{18}F-FDG metabolic volume and cold-induced ^{18}F-FDG metabolic volume of *Nppa*$^{+/+}$ and *Nppa*$^{-/-}$ mice at RT and during cold exposure (n = 4).

(K) Muscle ^{18}F-FDG uptake of *Nppa*$^{+/+}$ and *Nppa*$^{-/-}$ mice at RT and during cold exposure (n = 4).

Results are shown as mean ± SEM. *p < 0.05, **p < 0.01, ***p < 0.001, and ****p < 0.0001.

orchestrating the transcriptional program for substrate oxidation and thermogenesis in BAT (Puigserver et al., 1998). Brown fat lipid accumulation in *Nppa*$^{-/-}$ mice seems to occur independently of changes in NEFA transport through *Cd36* (Figure 2G) and lipoprotein lipase (*Lpl*) (Figure 2H) gene expression, which were similarly induced by cold exposure in both genotypes. In the same line, no change in protein content of the rate-limiting enzymes ATGL (Figure 2I) and HSL (Figure 2J), as well as *de novo* lipogenesis genes such as carbohydrate responsive-element binding protein-β (*Chrebpβ*), acetyl-coA carboxylase 1 (*Acc1*), and FA synthase (*Fas*) (Figures S2D–S2F) were noted in *Nppa*$^{-/-}$ versus wild-type control. Reduced cold-induced BAT activation and glucose uptake were associated with a significant increase of cold-induced *Glut1* expression (Figure S2G), while no

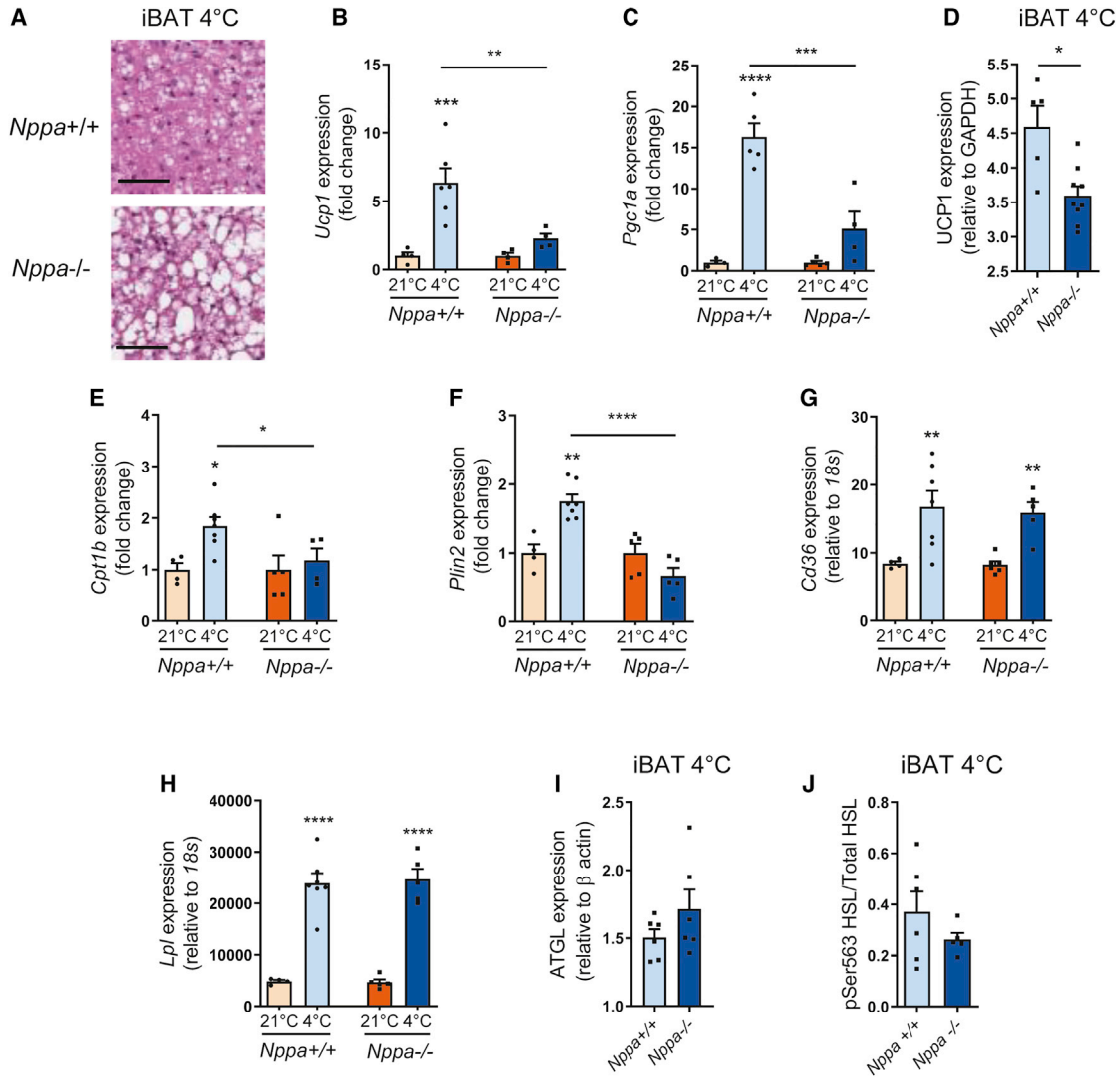

Figure 2. ANP Deficiency Induces BAT Morphological and Molecular Changes

(A) Representative hematoxylin and eosin staining of interscapular BAT (iBAT) sections of *Nppa*$^{+/+}$ and *Nppa*$^{-/-}$ mice after cold exposure. Scale bar, 50 μm.
(B and C) Relative mRNA levels of *Ucp1* (B) and *Pgc1α* (C) in iBAT from *Nppa*$^{+/+}$ (n = 4) and *Nppa*$^{-/-}$ (n = 6) mice housed at RT or after cold exposure.
(D) Relative UCP1 protein content in iBAT of *Nppa*$^{+/+}$ (n = 5) and *Nppa*$^{-/-}$ (n = 9) mice after cold exposure.
(E–H) Relative mRNA levels of *Cpt1b* (E), *Plin2* (F), *Cd36* (G), and *Lpl* (H) in iBAT from *Nppa*$^{+/+}$ (n = 5) and *Nppa*$^{-/-}$ (n = 7) mice housed at RT or after cold exposure.
(I) Relative ATGL protein content in iBAT of *Nppa*$^{+/+}$ and *Nppa*$^{-/-}$ mice after cold exposure (n = 6).
(J) Relative pS563 HSL protein content in iBAT of *Nppa*$^{+/+}$ (n = 6) and *Nppa*$^{-/-}$ (n = 5) mice after cold exposure.
Results are shown as mean ± SEM. *p < 0.05, **p < 0.01, ***p < 0.001, and ****p < 0.0001.

change in *Glut4* (Figure S2H) was observed in *Nppa*$^{-/-}$ mice. Of note, acute changes in Glut1 mRNA were not associated with significant changes in total GLUT1 protein in BAT of cold-exposed mice (Figure S2I). Finally, all observed differences of cold-induced gene expression in Nppa$^{-/-}$ mice appeared independent of changes in BAT mitochondrial respiration measured *ex vivo* in isolated mitochondria (Figure S2J).

Collectively, ANP deficiency causes marked morphological and cellular alterations of BAT biology and impairs cold-induced thermogenic genes activation which seems independent of changes in FA uptake and triglycerides (TG) hydrolysis.

ANP Is Required for Beige Adipocyte Recruitment during Acute Cold Exposure

Previous studies have shown that the ratio of GCA to NPRC expression determines cardiac NP biological activity in human and mice adipose tissue (AT) (Coué et al., 2015, 2018; Kovacova et al., 2016; Rydén et al., 2016). Thus, genetic ablation of adipose NPRC increases NP signaling through GCA in mice (Bordicchia et al., 2012). Here, we show that acute cold exposure induces WAT changes in NP receptor expression compared to mice housed at thermoneutral temperature in a depot-specific manner. Acute cold exposure upregulated the ratio of GCA to

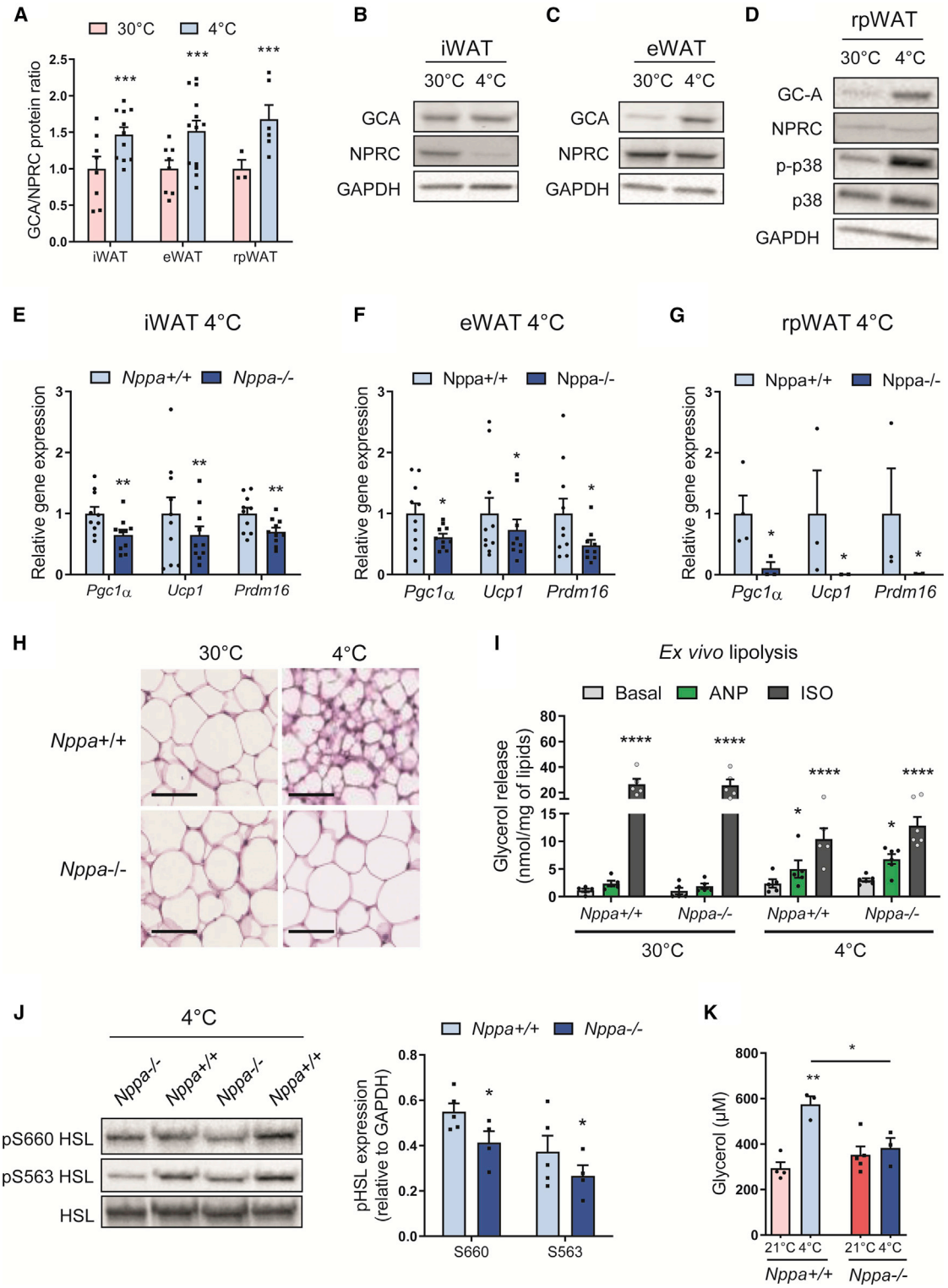

Figure 3. ANP Is Required for Beige Adipocyte Recruitment and Lipolysis during Acute Cold Exposure

(A) GCA-to-NPRC protein ratio in iWAT, eWAT, and rpWAT of WT mice housed at thermoneutral temperature (30°C) (n = 8) or after acute cold exposure (5 h at 4°C) (n = 13).

(B and C) Representative immunoblot of GC-A, NPRC and GAPDH in iWAT (B) and eWAT (C) of WT mice housed at 30°C or after acute cold exposure.

(D) Representative immunoblot of GC-A, NPRC, p-p38, p38, and GAPDH in rpWAT of WT mice housed at 30°C or after acute cold exposure.

(legend continued on next page)

NPRC mRNA (Figure S3A) and protein expression (Figure 3A) in the three WAT depots tested. As previously described (Bordicchia et al., 2012), we noted that NPRC protein was significantly diminished in iWAT (Figures 3B and S3B), while GCA protein remained unchanged (Figures 3B and S3C). Conversely, acute cold exposure upregulated GCA protein expression specifically in epididymal WAT (eWAT) (Figures 3C and S3C) and retroperitoneal WAT (rpWAT) (Figure 3D), while NPRC remained unaffected (Figures 3C, 3D, and S3B). Of interest, increased *Gca* gene expression was also observed in primary mouse adipocytes exposed to cold in culture (31°C) (Figure S3D), while *Nprc* remained unchanged (Figure S3E), demonstrating a cell-autonomous increase of the GCA-to-NPRC ratio in cold-exposed white adipocytes (Figure S3F). Cold-induced upregulation of GCA-to-NPRC ratio coincided with a sharp increase of p38 MAPK phosphorylation (Figure S3D) and robust induction of its downstream transcriptional targets, UCP1 and PGC1α, in iWAT (Figure S3G), eWAT (Figure S3H), rpWAT (Figure S3I), and iBAT (Figure S3J). The induction of beige adipocytes in WAT, the so-called browning/beigeing process, is highly adipose depot dependent in mice (Frontini and Cinti, 2010; Ohno et al., 2012). iWAT and rpWAT undergo the most profound induction of UCP1 (>30-fold), whereas eWAT exhibits a weak response (<10-fold). Cold-induced transcriptional activation of thermogenic genes was suppressed by ~40% in iWAT (Figure 3E) and eWAT (Figure 3F) and severely impaired in rpWAT (Figure 3G) of ANP null mice compared to wild-type mice. The GCA-to-NPRC mRNA ratio was robustly induced in all WAT depots, with a more pronounced induction in rpWAT (~24-fold) compared to iWAT (~1.75-fold) and eWAT (~2.25-fold) upon cold exposure (Figure S3K). Moreover, rpWAT is sensitive to browning (Jankovic et al., 2015) and anatomically close to the kidneys, one main physiological site of action of ANP (Kuhn, 2016). Thus, our data show that ANP-induced thermogenic gene expression is WAT depot dependent, with rpWAT being the most responsive depot. Along with PGC1α and UCP1, we observed a significant reduction of PR domain containing 16 (PRDM16) mRNA levels. The thermogenic activity of brown and beige adipocytes is conferred by a core gene program controlled by the master transcriptional regulator PRDM16 shown to physically interact with PGC1α to transactivate UCP1 transcription (Seale et al., 2007). Consistent with cold-induced thermogenic gene expression, wild-type mice exposed to acute cold showed augmented iWAT thermogenic gene expression compared to mice housed at thermoneutrality, as evidenced by increased emergence of smaller adipocytes containing multilocular lipid droplets and hematoxylin and eosin (H&E) staining, a physiological response that was suppressed in ANP null mice (Figure 3H). Similarly to BAT, we did not find significant changes in the level of expression of cold-regulated genes involved in the control of beige adipocyte thermogenesis such as *β1ar* (Figure S3L), *β2ar* (Figure S3M), *β3ar* (Figure S3N), and *Serca2b* (Ikeda et al., 2017) (Figure S3O). No major change in genes involved in NP signaling and thermogenesis was observed in iWAT (Figures S4A and S4B) and eWAT (Figures S4C and S4D) at 30°C and 21°C between genotypes. No visual histomorphological differences in iWAT, eWAT, and rpWAT were noted at thermoneutrality (Figure S4E) and RT (Figure S4F) between $Nppa^{+/+}$ and $Nppa^{-/-}$ mice. Overall, our data emphasize that upon a physiological cold stress, cardiac ANP released significantly contributes to thermogenic adipocytes activation in WAT.

ANP Is Required for White Adipocyte Lipolysis during Acute Cold Exposure

Since acute exposure to 4°C upregulates the ratio of GCA to NPRC protein in WAT, we hypothesized that white adipocytes would become sensitive to ANP-induced lipolysis in cold conditions. Former studies indicated that murine adipocytes are resistant to the lipolytic effect of ANP (Sengenès et al., 2002), while genetic ablation of NPRC in mice restores a lipolytic effect of ANP (Bordicchia et al., 2012). Here, we demonstrate that acute cold exposure renders white adipocytes fully responsive to ANP-mediated lipolysis, whereas in mice housed at thermoneutral temperature, ANP shows no lipolytic effect as previously observed. Acute cold exposure increased ANP-mediated glycerol (Figure 3I) and NEFA (Figure S4G) release by 2- to 3-fold compared to basal conditions in adipocytes isolated from eWAT, while the effect of isoproterenol remained unchanged compared to thermoneutral temperature. The cold-mediated *ex vivo* WAT lipolytic capacity was comparable between wild-type and ANP null mice (Figure 3I). This is in agreement with the lack of change of GCA (Figure S4H) and NPRC (Figure S4I) protein expression in eWAT of ANP null versus wild-type mice, indicating no functional compensation. However, cold-exposed ANP null mice had a significant downregulation of HSL phosphorylation at Ser-660 and Ser-563 in eWAT (Figure 3J), two main activating sites targeted by both PKA and PKG in response to catecholamines and ANP stimulation (Sengenes et al., 2003). This suggests that the lack of ANP *in vivo* associates with a lower cold-induced activation of HSL in eWAT of ANP null mice. This translated into a severely defective cold-induced lipolysis in ANP knockout (KO) mice as reflected by the changes in plasma glycerol (Figure 3K) and NEFA (data not shown) concentrations between thermoneutral temperature and acute cold. Recent studies challenged the established view that intracellular lipolysis of lipid droplets inside BAT is rate limiting for non-shivering thermogenesis. Rather, these studies showed that WAT lipolysis

(E–G) Relative mRNA levels of *Pgc1a*, *Ucp1*, and *Prdm16* in iWAT (n = 10) (E), eWAT (n = 10) (F), and rpWAT (n = 3–5) (G) from $Nppa^{+/+}$ and $Nppa^{-/-}$ mice after acute cold exposure,

(H) Representative hematoxylin and eosinstaining of iWAT from $Nppa^{+/+}$ and $Nppa^{-/-}$ mice housed at 30°C or after cold exposure. Scale bar, 50 μm.

(I) *Ex vivo* adipocyte lipolysis in eWAT of $Nppa^{+/+}$ and $Nppa^{-/-}$ mice housed at 30°C or after acute cold exposure under basal, ANP (10 μM)-stimulated, and isoproterenol (1 μM)-stimulated conditions (n = 5).

(J) Representative immunoblot and quantitative bar graph of pS660 HSL, pS563 HSL, and HSL total protein in eWAT of $Nppa^{+/+}$ (n = 5) and $Nppa^{-/-}$ (n = 4) mice after cold exposure.

(K) Plasma glycerol levels of $Nppa^{+/+}$ (n = 5) and $Nppa^{-/-}$ (n = 3) mice housed at 30°C and after acute cold exposure.

Results are shown as mean ± SEM. *p < 0.05, **p < 0.01, ***p < 0.001, and ****p<0.0001.

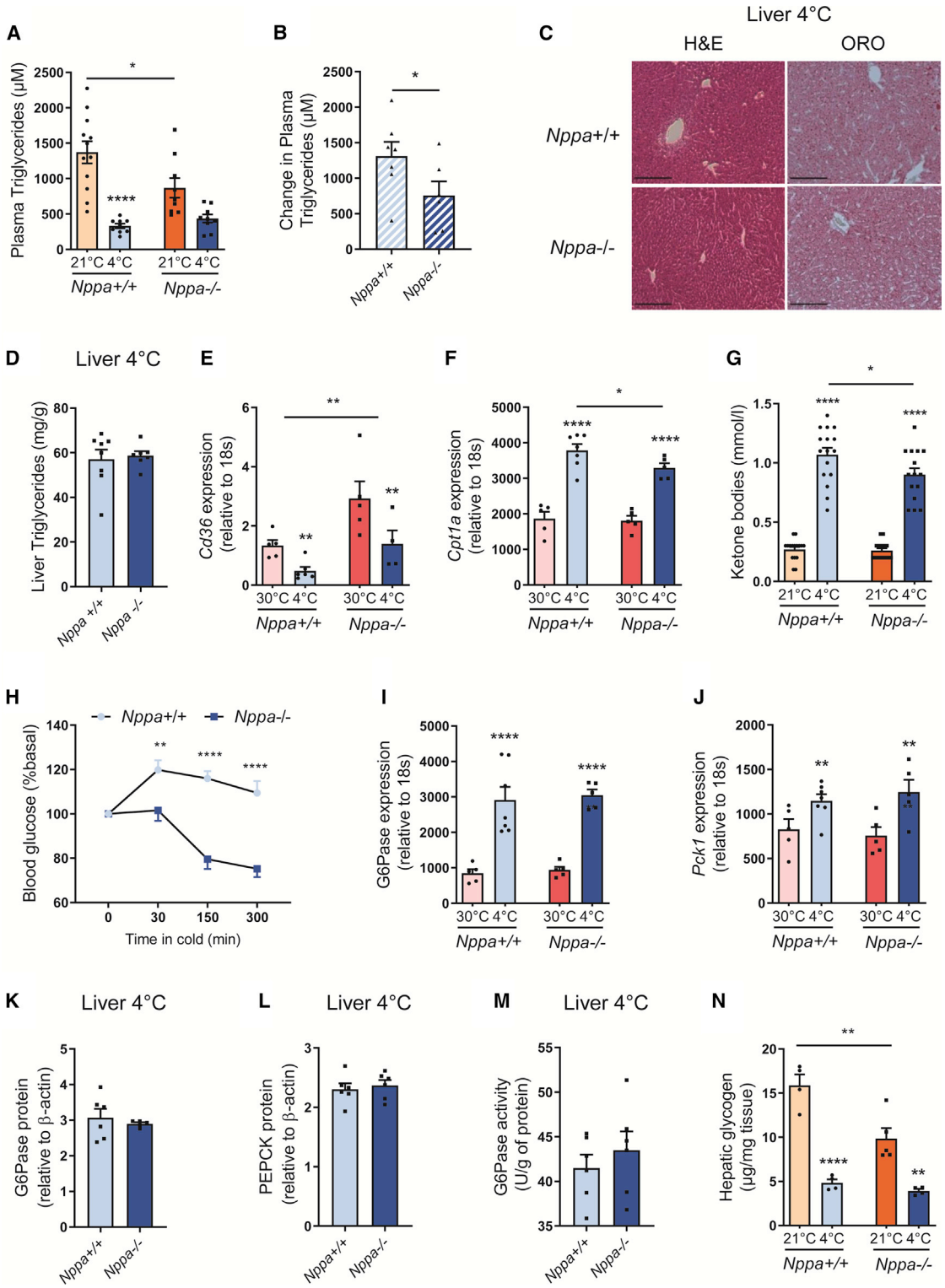

Figure 4. ANP Deficiency Impairs Plasma Triglycerides and Glucose Responses to Cold

(A) Plasma triglycerides levels of *Nppa*$^{+/+}$ (n = 12) and *Nppa*$^{-/-}$ (n = 9) mice housed at RT and after acute cold exposure.

(B) Change in plasma triglycerides levels of *Nppa*$^{+/+}$ (n = 7) and *Nppa*$^{-/-}$ (n = 6) mice housed at RT after acute cold exposure.

(C) Representative hematoxylin and eosin and oil red O (ORO) staining of liver from *Nppa*$^{+/+}$ and *Nppa*$^{-/-}$ mice after cold exposure. Scale bar, 200 μm.

(D) Liver triglycerides content of *Nppa*$^{+/+}$ (n = 8) and *Nppa*$^{-/-}$ (n = 7) mice after acute cold exposure.

(legend continued on next page)

is essential to fuel BAT with FA for heat production during fasting (Schreiber et al., 2017; Shin et al., 2017). Together, this suggests that the blunted cold-induced lipolytic response could contribute to the observed defective BAT activity and thermogenesis of ANP null mice. Altogether, our data stress that physiological release of ANP during cold exposure induces lipolysis to fuel BAT thermogenesis.

ANP Deficiency Impairs Plasma Triglycerides and Glucose Responses to Cold

Previous work suggested that besides NEFA, circulating TG and glucose are major substrates for BAT thermogenesis (Heine et al., 2018). In this study, we found reduced blood glucose levels upon cold exposure after 2 h (Figure S5A) while observing a time-dependent reduction of circulating insulin (Figure S5B) and circulating TG levels (Figure S5C) during a time course of cold exposure. We further observed decreased levels of circulating TG (Figure 4A) and a blunted cold-induced reduction of circulating plasma TG in *Nppa*$^{-/-}$ mice (Figure 4B). This occurred despite no significant difference in liver TG content between genotypes (Figures 4C and 4D). Lipolysis-derived NEFA availability is a major determinant of liver TG production (Samuel and Shulman, 2016). In line with a recent study (Simcox et al., 2017), hepatic genes related to lipid metabolism were strongly altered during cold exposure (Figures 4E, 4F, and S5D–S5G). Cold suppressed *Cd36* (Figure 4E) and *Pparα* (Figure S5D) mRNA levels while briskly inducing *Ppargc1a* (Figure S5E), *Atgl* (Figure S5F), and *Fgf21* (Figure S5G). Of interest, altered lipolysis in ANP-deficient mice was associated with a compensatory increase of liver *Cd36* gene expression (Figure 4E), while both liver *Cpt1a* mRNA levels (Figure 4F) and plasma ketone bodies levels (Figure 4G) were significantly reduced in *Nppa*$^{-/-}$ mice. This reveals a blunted NEFA utilization in the liver of ANP-deficient mice. In mirror of cold-induced NEFA utilization in liver, we observed a suppressed expression of *de novo* lipogenesis genes such as *Chrebp* (Figure S5H), *Acly* (Figure S5I), *Elovl3* (Figure S5J), and *Fas* (Figure S5K) that was similar in control and ANP-deficient mice.

Because lipolysis-derived NEFA availability is also a strong determinant of endogenous glucose production in mice (Perry et al., 2015), we investigated glucose metabolism in cold-exposed mice. Remarkably, ANP null mice were not able to maintain their blood glucose levels in a normal physiological range (Figure 4H). This phenomenon was independent of changes in glucose-6-phosphatase (*G6pase*) (Figure 4I) and phosphoenolpyruvate carboxy-kinase-1 (*Pck1*) (Figure 4J) mRNA levels, protein content (Figures 4K and 4L), and G6Pase activity (Figure 4M) in liver of ANP KO mice versus control. Importantly, we observed a sharp liver glycogen depletion upon acute cold exposure (~70%) in control mice (Figure 4N). Thus, total liver glycogen content was reduced by 38% in *Nppa*$^{-/-}$ mice compared to their wild-type littermates (Figure 4N), thus coinciding with the inability to maintain normal blood glucose levels during cold exposure. In summary, our data together indicate that ANP deficiency impairs liver TG and glycogen metabolism, thus contributing to reduced substrate availability to fuel BAT thermogenesis.

Cold Induces ANP and GC-A Is Associated with Brown/Beige Thermogenic Markers in Human Subcutaneous Abdominal WAT in Humans

To further examine if ANP could play a role in cold-induced activation of BAT in humans, we determined circulating plasma NP levels in human volunteers exposed to mild cold. Thus, recent studies using ^{18}F-FDG PET/CT revealed that acute cold exposure readily activates BAT in humans (Blondin et al., 2017; van Marken Lichtenbelt et al., 2009); however, the physiological cues orchestrating human BAT (hBAT) activation are still unclear. In a study in which 1-h cold exposure at 16°C increased mean blood pressure, BAT activity, and systemic lipolysis in lean healthy male volunteers (Figure 5A) (Vosselman et al., 2015), we measured a significant increase of plasma ANP levels by 1.7-fold (Figure 5B), whereas plasma BNP concentrations remained strictly unchanged (Figure 5C). In light of the previous findings in human primary BAT-derived adipocytes, this suggests that ANP is a cold-induced endocrine activator of BAT function in humans. Thus, in agreement with mice data, this implies that ANP behaves as the physiological endocrine ligand of GCA in response to cold stress in humans.

There is a large variability of white fat browning/beigeing in human individuals, particularly those with obesity (Coué et al., 2018). We next investigated the relationship between mRNA levels of GCA and markers of browning/beigeing in subcutaneous abdominal AT in a cohort of middle-aged individuals with a wide range of body mass index selected for a high baseline expression of UCP1 (n = 79). Correlation matrix analysis revealed that GCA was highly correlated with previously reported brown/beige-specific markers involved in mitochondrial oxidative metabolism, mitochondrial biogenesis, glucose, and FA metabolism (Coué et al., 2018) (Figure 5D). An optimal reordering of the correlation matrix based on hierarchical clustering revealed that *GCA* clustered with several brown/beige-specific gene markers such as *PPARα*, sirtuin 3 (*SIRT3*), carbonic anhydrase 4 (*CA4*), forkhead box K2 (*FOXK2*), and PPARγ co-activator 1β (*PPARGC1B*) (dotted line box, Figure 5D). The top-ranking genes displaying the highest correlations with *GCA* were the beige-specific marker *CA4* (Figure 5E), the lipid droplet-associated protein perilipin 5 (*PLIN5*) (Figure 5F), the transcription factor

(E and F) Relative mRNA levels of *Cd36* (E) and *Cpt1a* (F) in iBAT from *Nppa*$^{+/+}$ and *Nppa*$^{-/-}$ mice housed at 30°C or after cold exposure (n = 5).
(G) Plasma ketone bodies levels of *Nppa*$^{+/+}$ and *Nppa*$^{-/-}$ mice housed at RT and after acute cold exposure (n = 16).
(H) Change in blood glucose from baseline in *Nppa*$^{+/+}$ (n = 13) and *Nppa*$^{-/-}$ (n = 10) mice during 5-h cold exposure.
(I and J) Relative mRNA levels of *G6Pase* (I) and *Pck1* (J) in liver from *Nppa*$^{+/+}$ and *Nppa*$^{-/-}$ mice housed at 30°C (n = 5) or after cold exposure (n = 7).
(K and L) Relative G6Pase (K) and PEPCK (L) protein content in liver of *Nppa*$^{+/+}$ and *Nppa*$^{-/-}$ mice after cold exposure (n = 6).
(M) G6Pase activity in liver of *Nppa*$^{+/+}$ and *Nppa*$^{-/-}$ mice after cold exposure (n = 6).
(N) Hepatic glycogen content in liver of *Nppa*$^{+/+}$ and *Nppa*$^{-/-}$ mice housed at RT (n = 5) or after cold exposure (n = 4).
Results are shown as mean ± SEM. *p < 0.05, **p < 0.01, and ****p < 0.0001.

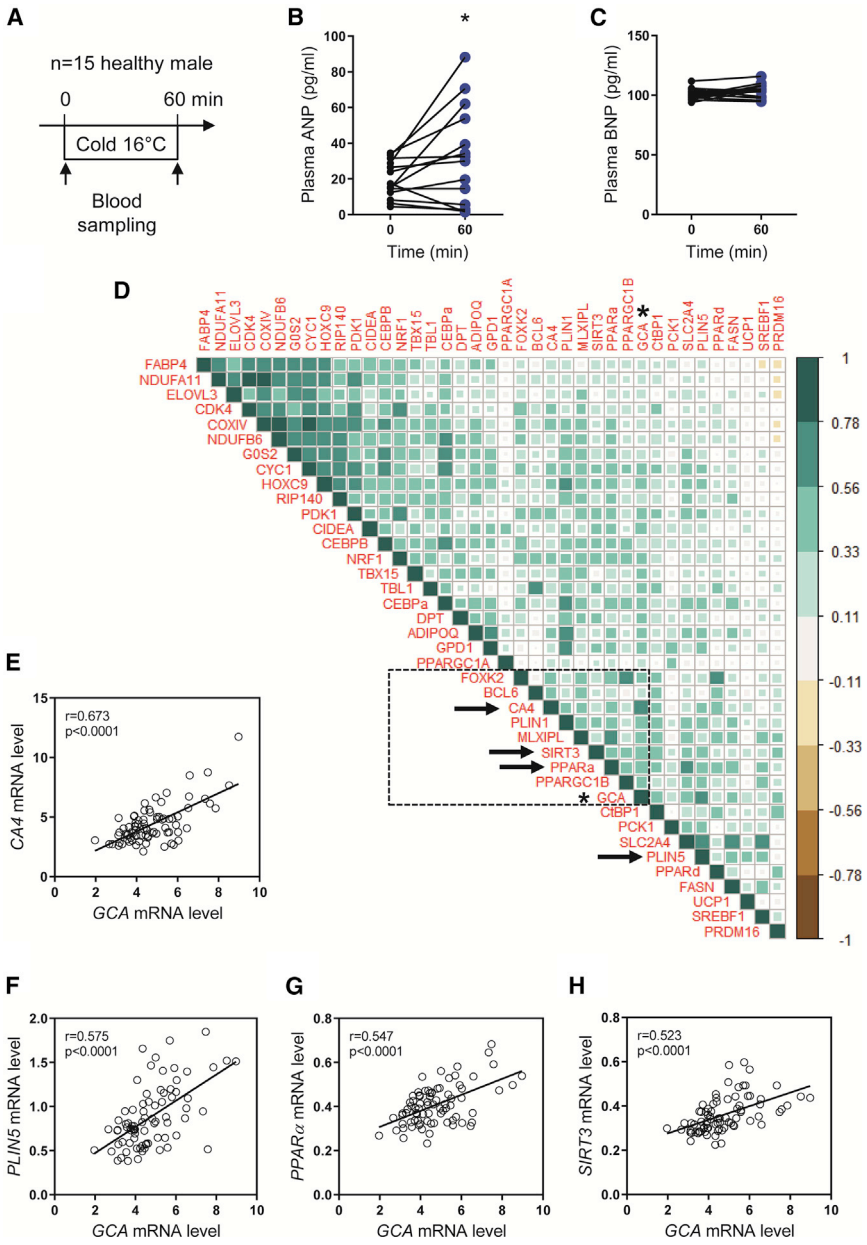

Figure 5. GC-A Is Associated with Brown/Beige and Thermogenic Markers in Human Subcutaneous Abdominal WAT

(A) Study design of acute cold exposure in human healthy volunteers.

(B) Plasma ANP levels in human healthy volunteers before and after 60-min cold exposure (n = 14).

(C) Plasma BNP levels in human healthy volunteers before and after 60-min cold exposure (n = 15).

(D) Correlation matrix of the 39 brown/beige-specific gene markers significantly correlated with *GCA*. Color intensity and spread are directly proportional to correlation coefficients as shown by the vertical scale. The dot line boxplot indicates a gene cluster containing GCA (indicated by an asterisk).

(E–H) Univariate linear regression between *GCA* mRNA level and *CA4* (E), *PLIN5* (F), *PPARα* (G), and *SIRT3* (H) mRNA levels in human WAT (n = 79).

*p < 0.05 versus time point 0.

PPARα (Figure 5G), and the brown-specific mitochondrial *SIRT3* (Figure 5H), all genes highly expressed in BAT and involved in metabolic pathways supporting thermogenic function (Coué et al., 2018). Thus, correlations between *GCA* and brown/beige-specific markers support a role for ANP/GCA signaling in bona fide thermogenic adipocytes of human subcutaneous abdominal WAT.

ANP Activates Mitochondrial Uncoupling in BAT and a Thermogenic Program in Human Primary Brown/Beige and White Adipocytes

^{18}F-FDG PET/CT revealed the existence of active BAT in the supraclavicular and neck areas of adult humans that can be readily activated by cold exposure (Cypess et al., 2009; van Marken Lichtenbelt et al., 2009; Nedergaard et al., 2007; Virtanen et al., 2009). It was suggested that these hBAT depots are in fact composed of UCP1-positive adipocytes bearing a transcriptional signature of beige rather than brown adipocytes as found in rodents (Wu et al., 2012).

Here, we differentiated adipocytes derived from hBAT (prevertebral) or hWAT (neck) *in vitro* from the same subject using four independent donors as previously described (Broeders et al., 2015; Wu et al., 2012). mRNA expression levels of *UCP1*, *PRDM16*, cell-death-inducing DFFA-like effector A (*CIDEA*), and nuclear respiratory factor 1 (*NRF1*) were significantly higher in brown/beige compared to white adipocytes (Figure S6A). Thus, we also observed a higher gene expression level of the NP-signaling components *NPRC*, *PRKGI*, and phosphodiesterase 5A *(PDE5A)* in BAT biopsy-derived adipocytes (Figure S6B). We next measured mitochondrial oxygen consumption under ATP synthase inhibition by oligomycin treatment to focus on mitochondrial uncoupled respiration (state 4). We have previously shown that β-adrenergic stimulation leads to pronounced mitochondrial uncoupling in human primary brown/beige adipocytes, which is markedly less in human primary white adipocytes, illustrating the unique feature of human adipocytes derived from the neck region (Broeders et al., 2015). Interestingly, we here show that ANP dose-dependently activates uncoupled mitochondrial respiration to ~50% of the effect of norepinephrine (NE) in human brown/beige adipocytes (Figures 6A and 6B). This effect was markedly lower in WAT-derived adipocytes (Figures 6C and 6D). ANP at the lowest dose of 100 nM nearly doubled maximal uncoupled respiration measured under carbonilcyanide

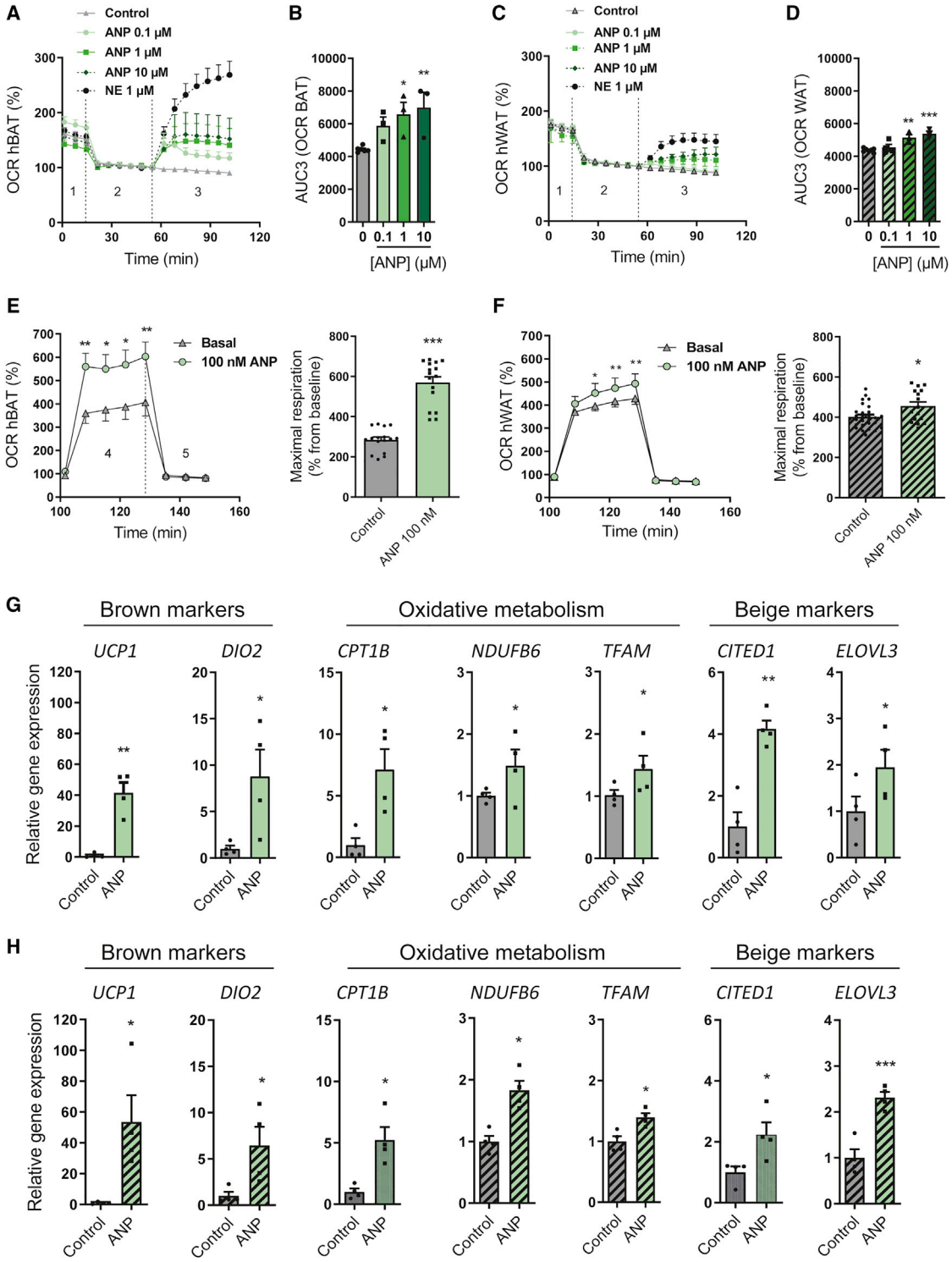

Figure 6. ANP Activates Mitochondrial Uncoupling in BAT and a Thermogenic Program in Human Primary Brown/Beige and White Adipocytes

(A) Oxygen consumption rate (OCR) of human primary brown/beige adipocytes (hBATs) in the absence (control) or presence of ANP (0.1 μM, 1 μM, or 10 μM) and NE (1 μM) for 3 h (n = 4). 1, basal respiration; 2, oligomycin; 3, treatments with different doses of ANP and NE.

(B) Area under the curve (AUC) of treatment-induced OCR calculated during phase 3 (uncoupled respiration during oligomycin inhibition of ATP synthase) in (A).

(C) OCR of human primary white adipocytes WAT (hWAT) in the absence (control) (n = 6) or presence of ANP (0.1 μM, 1 μM, or 10 μM) and NE (1 μM) for 3 h (n = 4). 1, basal respiration; 2, oligomycin; 3, treatments with different doses of ANP and NE.

(legend continued on next page)

p-triflouromethoxyphenylhydrazone (FCCP) in human brown/beige adipocytes (Figure 6E). A similar but weaker effect was observed in hWAT adipocytes (Figure 6F). This reveals that ANP can directly activate mitochondrial uncoupling and respiration in human primary brown/beige adipocytes. We next examined if ANP could induce a transcriptional thermogenic program in human brown/beige and white primary adipocytes as observed *in vivo* in mice. ANP treatment briskly increased mRNA levels of *UCP1* both in human WAT and BAT adipocytes (Figure S6C). A peak was observed after 3-h treatment with levels returning to baseline after 48 -h and 72-h treatment for *UCP1* and *CPT1B* in human brown/beige adipocytes (Figures S6D and S6E) and white (Figures S6F and S6G) adipocytes. Interestingly, acute treatment (3 h) with ANP at 100 nM increased to a variable degree (from 1.5- to 50-fold) a number of brown markers (e.g., *UCP1* and deiodinase type 2 [*DIO2*]), beige markers (e.g., Cbp/P300 interacting transactivator with Glu/Asp-rich C-terminal domain 1 [*CITED1*] and elongation of very long chain FAs protein 3 [*ELOVL3*]), and mitochondrial oxidative metabolism markers (*CPT1B*, NADH:ubiquinone oxidoreductase subunit B6 ([*NDUFB6*]), and transcription factor A, mitochondrial [*TFAM*]) in brown/beige adipocytes (Figure 6G) and white adipocytes (Figure 6H). Taken together, these results indicate that ANP has the capacity to activate a thermogenic program in human primary brown/beige and white adipocytes, and mitochondrial uncoupling in brown/beige adipocytes. This implies that ANP mimetics and/or pharmacological compounds able to increase ANP/GCA signaling may be attractive strategies to activate BAT in humans.

DISCUSSION

The current classical view in mammals is that brown/beige fat is primarily activated by norepinephrine released from sympathetic nerves upon cold exposure. However, the fact that the nonselective β-agonist isoproterenol fails to activate BAT in humans (Vosselman et al., 2012), combined with the observation that the β_3-adrenergic receptor is dispensable for cold-induced thermogenic gene activation in mice (de Jong et al., 2017), points toward the existence of alternative non-adrenergic regulatory systems that control BAT activation and function in response to cold. We here show that ANP, a cardiac hormone controlling blood volume and pressure, is required for cold-induced brown/beige adipocyte activation.

Previous work demonstrated that ANP contributes to cold-induced diuresis in healthy humans (Hassi et al., 1991). In response to cold, contraction of superficial blood vessels will limit heat loss, and as a consequence, blood will be shunted away toward deeper large blood vessels that will increase cardiac filling pressure of the right atrium (i.e., increased cardiac preload). As a result, ANP secretion will be induced to normalize the increase in cardiac preload by enhancing diuresis. Herein, we demonstrate that ANP released upon cold exposure, but not BNP, will activate BAT to produce heat and maintain euthermia. BNP, the product of *Nppb*, is marginally expressed in the right atria of the heart compared to ANP (Kuhn, 2016). This likely explains why cardiac BNP expression and circulating levels are poorly affected by changes in cardiac filling pressure such as induced by cold exposure in this study.

In previous studies, the complete lack of all three β-adrenergic receptors (β-less mice) (Bachman et al., 2002) or sympathetic innervations in WAT through pharmacological ablation by 6-hydroxydopamine (Rohm et al., 2016) or genetic invalidation of tyrosine kinase receptor A (Jiang et al., 2017) was shown to suppress partially but not completely cold-induced UCP1 expression. Although β-less mice develop hypothermia, it is still unclear to what extent BAT activity is hampered by the lack of β-adrenergic receptors. In this study, we show using ^{18}F-FDG PET/CT that the lack of ANP abrogates approximately half of BAT ^{18}F-FDG glucose uptake and >60% of transcriptional activation of *Ucp1* and *Pgc1α* in BAT in response to acute cold exposure. The accumulation of multiple lipid droplets in cold-exposed BAT (i.e., BAT steatosis) of ANP null mice is a sign of dysfunctional BAT, as observed in other mouse models (Bachman et al., 2002; Seale et al., 2007; Simcox et al., 2017). A failure to adequately activate BAT and UCP1 in ANP-deficient mice will lead to fat storage within lipid droplets in face of increased FA supply. This accumulation of multiple lipid droplets in BAT of ANP null mice is not observed at RT for which the cold stress represents a too-moderate challenge to unmask prototypical BAT-related phenotypes.

Recent studies indicate that BAT activation upon cold exposure is intimately linked to WAT lipolysis in fasted mice (Ikeda et al., 2017; Simcox et al., 2017), thus highlighting the need for a thermogenic factor to activate lipolysis. Although ANP is a powerful lipolytic hormone in human adipocytes, previous studies could not reveal a lipolytic effect of ANP in mouse adipocytes (Sengenès et al., 2002). We here reconcile these studies, demonstrating that cold exposure briskly increases ANP receptor GCA gene and protein expression in WAT, thus rendering mouse adipocytes responsive to ANP-mediated lipolysis. Importantly, we here demonstrate a cell-autonomous upregulation of GCA in primary mouse WAT adipocytes cultured at 31°C instead of 37°C. This indicates that acute cold is sufficient to upregulate GCA expression in white adipocytes independently of systemic neuroendocrine factors. We next show that cold-induced systemic lipolysis, reflected by increased plasma glycerol levels and HSL activation by phosphorylation in eWAT, is blunted in ANP null mice.

Besides NEFA derived from WAT lipolysis, circulating TGs have been shown as major BAT substrates during cold exposure (Heine

(D) AUC of treatment-induced OCR calculated during phase 3 in (uncoupled respiration during oligomycin inhibition of ATP synthase) (C).
(E) Maximal OCR (induced by FCCP) of hBAT in absence (control) or presence of ANP 100 nM (n = 4 independent donors). 4, FCCP; 5, rotenone and antimycin A.
(F) Maximal OCR (induced by FCCP) of hWAT in absence (control) or presence of ANP 100 nM (n = 4 independent donors). 4, FCCP; 5, rotenone and antimycin A.
(G) Relative mRNA levels of brown (*UCP1* and *DIO2*), brown/beige (*CPT1B*, *NDUFB6*, and *TFAM*), and beige (*CITED1* and *ELOVL3*) markers in hBAT in the absence (control) or presence of ANP 100 nM (n = 4).
(H) Relative mRNA levels of brown (*UCP1* and *DIO2*), brown/beige (*CPT1B*, *NDUFB6*, and *TFAM*), and beige (*CITED1* and *ELOVL3*) markers in hWAT in the absence (control) or presence of ANP 100 nM (n = 4).
Results are shown as mean ± SEM. *p < 0.05, **p < 0.01, and ***p < 0.001 versus control.

et al., 2018). We here unravel a strong defect in plasma TG production and/or utilization in *Nppa*$^{-/-}$ mice during cold exposure despite a robust induction of *Lpl* in BAT of cold-exposed *Nppa*$^{-/-}$ mice similar to control littermates. In line with a recent study (Simcox et al., 2017), we observed drastic changes in expression of lipid metabolism genes in liver of cold-exposed mice. Cold exposure turns on FA oxidative gene networks while downregulating lipid synthesis gene programs such as *de novo* lipogenesis. This leads to substantial FA utilization by the liver thus producing ketone bodies. Remarkably, cold-induced upregulation of *Cpt1a*, a rate-limiting enzyme in mitochondrial FA oxidation, and ketone bodies production was impaired in *Nppa*$^{-/-}$ mice. This together with a reduced cold-induced lipolysis in *Nppa*$^{-/-}$ mice largely contributes to this observed hepatic phenotype.

Previous works also highlighted that glucose is an important substrate for BAT during cold exposure in mice (Heine et al., 2018) and humans (Ouellet et al., 2012). Of importance, we observed that *Nppa*$^{-/-}$ mice fail to maintain their blood glucose levels during acute cold exposure when compared to wild-type mice. This effect appears independent of changes in protein content and enzyme activity of PEPCK and G6Pase, which are rate-limiting enzymes in hepatic glucose production. Thus, this could be reasonably explained by a reduced glycogenolysis during cold exposure due to reduced liver glycogen content in *Nppa*$^{-/-}$ mice. In addition, a blunted ANP-mediated lipolysis in WAT during cold exposure reduces NEFA availability and therefore liver endogenous glucose production (Perry et al., 2015). Our findings are consistent with a previous study, which showed a stimulatory effect of ANP on gluconeogenesis in perfused rat livers (Rashed et al., 1992). Thus, the lack of ANP could result in a blunted gluconeogenesis in cold-exposed mice. Collectively, a reduced availability and utilization of circulating NEFA, ketone bodies, TG, and glucose may largely contribute to impair BAT thermogenesis in cold-exposed *Nppa*$^{-/-}$ mice.

In summary, we identify cardiac ANP as a physiological endocrine activator of non-shivering thermogenesis in mammals. These data uncover an intriguing evolutionary interconnection between cardiac activity and non-shivering thermogenesis. While the sympathetic nervous system remains the best-known mediator of cold-induced thermogenesis and BAT recruitment in mammals, our findings shed light on alternative pathways that have been conserved across species to maintain euthermia. They may open the path to potential pharmacological strategies targeted to enhance ANP/GCA signaling for human BAT recruitment to improve metabolic profile in individuals with obesity and type 2 diabetes.

STAR★METHODS

Detailed methods are provided in the online version of this paper and include the following:

- KEY RESOURCES TABLE
- RESOURCE AVAILABILITY
  - Lead Contact
  - Materials Availability
  - Data and Code Availability
- EXPERIMENTAL MODEL AND SUBJECT DETAILS
  - Clinical studies and human subjects
  - Mice
  - Human primary adipocytes culture
  - Mouse primary adipocytes culture
- METHOD DETAILS
  - Blood analyses
  - Echocardiography
  - ^{18}F-FDG PET/CT
  - Cellular cooling
  - Adipocyte lipolysis
  - Histology
  - Immunofluorescence
  - Hepatic glycogen content
  - Hepatic triglycerides content
  - Mitochondrial respiration
  - SeaHorse
  - Real-time qPCR
  - Western blot
- QUANTIFICATION AND STATISTICAL ANALYSIS

SUPPLEMENTAL INFORMATION

Supplemental Information can be found online at https://doi.org/10.1016/j.celrep.2020.108075.

ACKNOWLEDGMENTS

This work was supported by grants from INSERM, Société Francophone du Diabète, and the European Foundation for the Study of Diabetes (C.M.) and the Commission of the European Communities (FP6-513946 DiOGenes and HEALTH-F2-2011-278373 DIABAT) (D. Lagarde). D.C. is supported by a PhD fellowship from INSERM/Occitanie Region. We are very grateful to Caroline Nevoit, Sarah Gandarillas, and Candy Escassut (CREFRE) for technical assistance in PET/CT imaging. We also thank Alexandre Lucas (APC core facility), Frédéric Martins (GET-TQ core facility), Lucie Fontaine (Histology core facility), and Dr. Jean-Philippe Pradère and Enzo Piccolo (Liver ORO staining) for their technical support. D.L. is a member of Institut Universitaire de France. We warmly acknowledge Pr. Max Lafontan for critical reading of the manuscript.

AUTHOR CONTRIBUTIONS

Conceptualization, D.C. and C.M.; Methodology, D.C. and C.M.; Investigation, D.C., M.C., E.B.M.N., V.B., D.A.L., C.P., C.L., J.V.P., M.S., L.M., M.-A.M., Y.J., Y.S.-M., A.M., S.D., G.T., N.V., V.B., F.L., A.C., W.H.M.S., and A.A.; Resources, G.M., W.v.M.L., P.S., D.L.; Writing – Original Draft, D.C. and C.M.; Writing – Review & Editing, D.C., E.B.M.N., A.C., L.C., G.M., W.v.M.L., P.S., D.L., and C.M.; Supervision, D.C. and C.M.; Funding Acquisition, D.L. and C.M.

DECLARATION OF INTERESTS

The authors declare no competing interests.

Received: May 31, 2018
Revised: February 12, 2020
Accepted: August 5, 2020
Published: August 25, 2020

REFERENCES

Bachman, E.S., Dhillon, H., Zhang, C.Y., Cinti, S., Bianco, A.C., Kobilka, B.K., and Lowell, B.B. (2002). betaAR signaling required for diet-induced thermogenesis and obesity resistance. Science *297*, 843–845.

Barquissau, V., Léger, B., Beuzelin, D., Martins, F., Amri, E.-Z., Pisani, D.F., Saris, W.H.M., Astrup, A., Maoret, J.-J., Iacovoni, J., et al. (2018). Caloric restriction and diet-induced weight loss do not induce browning of human subcutaneous white adipose tissue in women and men with obesity. Cell Rep. *22*, 1079–1089.

Blondin, D.P., Tingelstad, H.C., Noll, C., Frisch, F., Phoenix, S., Guérin, B., Turcotte, E.E., Richard, D., Haman, F., and Carpentier, A.C. (2017). Dietary fatty acid metabolism of brown adipose tissue in cold-acclimated men. Nat. Commun. *8*, 14146.

Bordicchia, M., Liu, D., Amri, E.Z., Ailhaud, G., Dessì-Fulgheri, P., Zhang, C., Takahashi, N., Sarzani, R., and Collins, S. (2012). Cardiac natriuretic peptides act via p38 MAPK to induce the brown fat thermogenic program in mouse and human adipocytes. J. Clin. Invest. *122*, 1022–1036.

Broeders, E.P., Nascimento, E.B., Havekes, B., Brans, B., Roumans, K.H., Tailleux, A., Schaart, G., Kouach, M., Charton, J., Deprez, B., et al. (2015). The bile acid chenodeoxycholic acid increases human brown adipose tissue activity. Cell Metab. *22*, 418–426.

Cannon, B., and Nedergaard, J. (2004). Brown adipose tissue: function and physiological significance. Physiol. Rev. *84*, 277–359.

Cao, W., Daniel, K.W., Robidoux, J., Puigserver, P., Medvedev, A.V., Bai, X., Floering, L.M., Spiegelman, B.M., and Collins, S. (2004). p38 mitogen-activated protein kinase is the central regulator of cyclic AMP-dependent transcription of the brown fat uncoupling protein 1 gene. Mol. Cell. Biol. *24*, 3057–3067.

Coué, M., Badin, P.M., Vila, I.K., Laurens, C., Louche, K., Marquès, M.A., Bourlier, V., Mouisel, E., Tavernier, G., Rustan, A.C., et al. (2015). Defective natriuretic peptide receptor signaling in skeletal muscle links obesity to type 2 diabetes. Diabetes *64*, 4033–4045.

Coué, M., Barquissau, V., Morigny, P., Louche, K., Lefort, C., Mairal, A., Carpéné, C., Viguerie, N., Arner, P., Langin, D., et al. (2018). Natriuretic peptides promote glucose uptake in a cGMP-dependent manner in human adipocytes. Sci. Rep. *8*, 1097.

Cypess, A.M., Lehman, S., Williams, G., Tal, I., Rodman, D., Goldfine, A.B., Kuo, F.C., Palmer, E.L., Tseng, Y.H., Doria, A., et al. (2009). Identification and importance of brown adipose tissue in adult humans. N. Engl. J. Med. *360*, 1509–1517.

de Jong, J.M.A., Wouters, R.T.F., Boulet, N., Cannon, B., Nedergaard, J., and Petrovic, N. (2017). The β_3-adrenergic receptor is dispensable for browning of adipose tissues. Am. J. Physiol. Endocrinol. Metab. *312*, E508–E518.

de la Rosa Rodriguez, M.A., and Kersten, S. (2017). Regulation of lipid droplet-associated proteins by peroxisome proliferator-activated receptors. Biochim. Biophys. Acta Mol. Cell Biol. Lipids *1862* (*10 Pt B*), 1212–1220.

Frontini, A., and Cinti, S. (2010). Distribution and development of brown adipocytes in the murine and human adipose organ. Cell Metab. *11*, 253–256.

Gnad, T., Scheibler, S., von Kügelgen, I., Scheele, C., Kilić, A., Glöde, A., Hoffmann, L.S., Reverte-Salisa, L., Horn, P., Mutlu, S., et al. (2014). Adenosine activates brown adipose tissue and recruits beige adipocytes via A2A receptors. Nature *516*, 395–399.

Harms, M., and Seale, P. (2013). Brown and beige fat: development, function and therapeutic potential. Nat. Med. *19*, 1252–1263.

Hassi, J., Rintamäki, H., Ruskoaho, H., Leppäluoto, J., and Vuolteenaho, O. (1991). Plasma levels of endothelin-1 and atrial natriuretic peptide in men during a 2-hour stay in a cold room. Acta Physiol. Scand. *142*, 481–485.

Heine, M., Fischer, A.W., Schlein, C., Jung, C., Straub, L.G., Gottschling, K., Mangels, N., Yuan, Y., Nilsson, S.K., Liebscher, G., et al. (2018). Lipolysis triggers a systemic insulin response essential for efficient energy replenishment of activated brown adipose tissue in mice. Cell Metab. *28*, 644–655.e4.

Ikeda, K., Kang, Q., Yoneshiro, T., Camporez, J.P., Maki, H., Homma, M., Shinoda, K., Chen, Y., Lu, X., Maretich, P., et al. (2017). UCP1-independent signaling involving SERCA2b-mediated calcium cycling regulates beige fat thermogenesis and systemic glucose homeostasis. Nat. Med. *23*, 1454–1465.

Jankovic, A., Golic, I., Markelic, M., Stancic, A., Otasevic, V., Buzadzic, B., Korac, A., and Korac, B. (2015). Two key temporally distinguishable molecular and cellular components of white adipose tissue browning during cold acclimation. J. Physiol. *593*, 3267–3280.

Jiang, Y., Berry, D.C., and Graff, J.M. (2017). Distinct cellular and molecular mechanisms for β3 adrenergic receptor-induced beige adipocyte formation. eLife *6*, e30329.

Kajimura, S., Spiegelman, B.M., and Seale, P. (2015). Brown and beige fat: physiological roles beyond heat generation. Cell Metab. *22*, 546–559.

Kovacova, Z., Tharp, W.G., Liu, D., Wei, W., Xie, H., Collins, S., and Pratley, R.E. (2016). Adipose tissue natriuretic peptide receptor expression is related to insulin sensitivity in obesity and diabetes. Obesity (Silver Spring) *24*, 820–828.

Kuhn, M. (2016). Molecular physiology of membrane guanylyl cyclase receptors. Physiol. Rev. *96*, 751–804.

Larsen, T.M., Dalskov, S.M., van Baak, M., Jebb, S.A., Papadaki, A., Pfeiffer, A.F., Martinez, J.A., Handjieva-Darlenska, T., Kunešová, M., Pihlsgård, M., et al.; Diet, Obesity, and Genes (Diogenes) Project (2010). Diets with high or low protein content and glycemic index for weight-loss maintenance. N. Engl. J. Med. *363*, 2102–2113.

Mallela, J., Ravi, S., Jean Louis, F., Mulaney, B., Cheung, M., Sree Garapati, U., Chinnasamy, V., Wang, C., Nagaraj, S., Mohapatra, S.S., and Mohapatra, S. (2013). Natriuretic peptide receptor A signaling regulates stem cell recruitment and angiogenesis: a model to study linkage between inflammation and tumorigenesis. Stem Cells *31*, 1321–1329.

Mandard, S., Müller, M., and Kersten, S. (2004). Peroxisome proliferator-activated receptor alpha target genes. Cell. Mol. Life Sci. *61*, 393–416.

Monteillet, L., Gjorgjieva, M., Silva, M., Verzieux, V., Imikirene, L., Duchampt, A., Guillou, H., Mithieux, G., and Rajas, F. (2018). Intracellular lipids are an independent cause of liver injury and chronic kidney disease in non alcoholic fatty liver disease-like context. Mol. Metab. *16*, 100–115.

Moro, C., Crampes, F., Sengenes, C., De Glisezinski, I., Galitzky, J., Thalamas, C., Lafontan, M., and Berlan, M. (2004). Atrial natriuretic peptide contributes to physiological control of lipid mobilization in humans. FASEB J. *18*, 908–910.

Nedergaard, J., and Cannon, B. (2010). The changed metabolic world with human brown adipose tissue: therapeutic visions. Cell Metab. *11*, 268–272.

Nascimento, E.B.M., Sparks, L.M., Divoux, A., van Gisbergen, M.W., Broeders, E.P.M., Jörgensen, J.A., Schaart, G., Bouvy, N.D., van Marken Lichtenbelt, W.D., and Schrauwen, P. (2018). Genetic Markers of Brown Adipose Tissue Identity and In Vitro Brown Adipose Tissue Activity in Humans, *26* (Obesity (Silver Spring), pp. 135–140.

Nedergaard, J., Bengtsson, T., and Cannon, B. (2007). Unexpected evidence for active brown adipose tissue in adult humans. Am. J. Physiol. Endocrinol. Metab. *293*, E444–E452.

Ohno, H., Shinoda, K., Spiegelman, B.M., and Kajimura, S. (2012). PPARγ agonists induce a white-to-brown fat conversion through stabilization of PRDM16 protein. Cell Metab. *15*, 395–404.

Ouellet, V., Labbé, S.M., Blondin, D.P., Phoenix, S., Guérin, B., Haman, F., Turcotte, E.E., Richard, D., and Carpentier, A.C. (2012). Brown adipose tissue oxidative metabolism contributes to energy expenditure during acute cold exposure in humans. J. Clin. Invest. *122*, 545–552.

Perry, R.J., Camporez, J.G., Kursawe, R., Titchenell, P.M., Zhang, D., Perry, C.J., Jurczak, M.J., Abudukadier, A., Han, M.S., Zhang, X.M., et al. (2015). Hepatic acetyl CoA links adipose tissue inflammation to hepatic insulin resistance and type 2 diabetes. Cell *160*, 745–758.

Planat-Benard, V., Silvestre, J.S., Cousin, B., André, M., Nibbelink, M., Tamarat, R., Clergue, M., Manneville, C., Saillan-Barreau, C., Duriez, M., et al. (2004). Plasticity of human adipose lineage cells toward endothelial cells: physiological and therapeutic perspectives. Circulation *109*, 656–663.

Puigserver, P., Wu, Z., Park, C.W., Graves, R., Wright, M., and Spiegelman, B.M. (1998). A cold-inducible coactivator of nuclear receptors linked to adaptive thermogenesis. Cell *92*, 829–839.

Rajas, F., Jourdan-Pineau, H., Stefanutti, A., Mrad, E.A., Iynedjian, P.B., and Mithieux, G. (2007). Immunocytochemical localization of glucose 6-phosphatase and cytosolic phosphoenolpyruvate carboxykinase in gluconeogenic

tissues reveals unsuspected metabolic zonation. Histochem Cell Biol *127*, 555–565.

Rashed, H.M., Nair, B.G., and Patel, T.B. (1992). Regulation of hepatic glycolysis and gluconeogenesis by atrial natriuretic peptide. Arch. Biochem. Biophys. *298*, 640–645.

Rohm, M., Schäfer, M., Laurent, V., Üstünel, B.E., Niopek, K., Algire, C., Hautzinger, O., Sijmonsma, T.P., Zota, A., Medrikova, D., et al. (2016). An AMP-activated protein kinase-stabilizing peptide ameliorates adipose tissue wasting in cancer cachexia in mice. Nat. Med. *22*, 1120–1130.

Rydén, M., Bäckdahl, J., Petrus, P., Thorell, A., Gao, H., Coue, M., Langin, D., Moro, C., and Arner, P. (2016). Impaired atrial natriuretic peptide-mediated lipolysis in obesity. Int. J. Obes. *40*, 714–720.

Samuel, V.T., and Shulman, G.I. (2016). The pathogenesis of insulin resistance: integrating signaling pathways and substrate flux. J. Clin. Invest. *126*, 12–22.

Schreiber, R., Diwoky, C., Schoiswohl, G., Feiler, U., Wongsiriroj, N., Abdellatif, M., Kolb, D., Hoeks, J., Kershaw, E.E., Sedej, S., et al. (2017). Cold-induced thermogenesis depends on ATGL-mediated lipolysis in cardiac muscle, but not brown adipose tissue. Cell Metab. *26*, 753–763–e7.

Seale, P., Kajimura, S., Yang, W., Chin, S., Rohas, L.M., Uldry, M., Tavernier, G., Langin, D., and Spiegelman, B.M. (2007). Transcriptional control of brown fat determination by PRDM16. Cell Metab. *6*, 38–54.

Sengenès, C., Berlan, M., De Glisezinski, I., Lafontan, M., and Galitzky, J. (2000). Natriuretic peptides: a new lipolytic pathway in human adipocytes. FASEB J. *14*, 1345–1351.

Sengenès, C., Zakaroff-Girard, A., Moulin, A., Berlan, M., Bouloumié, A., Lafontan, M., and Galitzky, J. (2002). Natriuretic peptide-dependent lipolysis in fat cells is a primate specificity. Am. J. Physiol. Regul. Integr. Comp. Physiol. *283*, R257–R265.

Sengenes, C., Bouloumie, A., Hauner, H., Berlan, M., Busse, R., Lafontan, M., and Galitzky, J. (2003). Involvement of a cGMP-dependent pathway in the natriuretic peptide-mediated hormone-sensitive lipase phosphorylation in human adipocytes. J. Biol. Chem. *278*, 48617–48626.

Shin, H., Ma, Y., Chanturiya, T., Cao, Q., Wang, Y., Kadegowda, A.K.G., Jackson, R., Rumore, D., Xue, B., Shi, H., et al. (2017). Lipolysis in brown adipocytes is not essential for cold-induced thermogenesis in mice. Cell Metab. *26*, 764–777.e5.

Simcox, J., Geoghegan, G., Maschek, J.A., Bensard, C.L., Pasquali, M., Miao, R., Lee, S., Jiang, L., Huck, I., Kershaw, E.E., et al. (2017). Global analysis of plasma lipids identifies liver-derived acylcarnitines as a fuel source for brown fat thermogenesis. Cell Metab. *26*, 509–522.e6.

van Marken Lichtenbelt, W.D., Vanhommerig, J.W., Smulders, N.M., Drossaerts, J.M., Kemerink, G.J., Bouvy, N.D., Schrauwen, P., and Teule, G.J. (2009). Cold-activated brown adipose tissue in healthy men. N. Engl. J. Med. *360*, 1500–1508.

Virtanen, K.A., Lidell, M.E., Orava, J., Heglind, M., Westergren, R., Niemi, T., Taittonen, M., Laine, J., Savisto, N.J., Enerbäck, S., and Nuutila, P. (2009). Functional brown adipose tissue in healthy adults. N. Engl. J. Med. *360*, 1518–1525.

Vosselman, M.J., van der Lans, A.A.J.J., Brans, B., Wierts, R., van Baak, M.A., Schrauwen, P., and van Marken Lichtenbelt, W.D. (2012). Systemic β-adrenergic stimulation of thermogenesis is not accompanied by brown adipose tissue activity in humans. Diabetes *61*, 3106–3113.

Vosselman, M.J., Hoeks, J., Brans, B., Pallubinsky, H., Nascimento, E.B., van der Lans, A.A., Broeders, E.P., Mottaghy, F.M., Schrauwen, P., and van Marken Lichtenbelt, W.D. (2015). Low brown adipose tissue activity in endurance-trained compared with lean sedentary men. Int. J. Obes. *39*, 1696–1702.

Wang, X., Minze, L.J., and Shi, Z.Z. (2012). Functional imaging of brown fat in mice with 18F-FDG micro-PET/CT. J. Vis. Exp. *69*, 4060.

Wei, T., and Simko, V. (2017). R package "corrplot": Visualization of a correlation matrix (Version 0.84). R Found. Stat. Comput., Vienna.. https://github.com/taiyun/corrplot

Wu, J., Boström, P., Sparks, L.M., Ye, L., Choi, J.H., Giang, A.-H., Khandekar, M., Virtanen, K.A., Nuutila, P., Schaart, G., et al. (2012). Beige adipocytes are a distinct type of thermogenic fat cell in mouse and human. Cell *150*, 366–376.

Yuan, K., Jin, X., Park, W.H., Kim, J.H., Park, B.H., and Kim, S.H. (2009). Modification of atrial natriuretic peptide system in cold-induced hypertensive rats. Regul. Pept. *154*, 112–120.

Zhang, F., Hao, G., Shao, M., Nham, K., An, Y., Wang, Q., Zhu, Y., Kusminski, C.M., Hassan, G., Gupta, R.K., et al. (2018). An adipose tissue atlas: an image-guided identification of human-like BAT and beige depots in rodents. Cell Metab. *27*, 252–262.e3.

STAR★METHODS

KEY RESOURCES TABLE

REAGENT or RESOURCE	SOURCE	IDENTIFIER
Antibodies		
Rabbit polyclonal anti-UCP1	Abcam	Cat# ab10983; RRID:AB_2241462
Rabbit polyclonal anti-NPRA (GC-A)	Abcam	Cat#ab154266
Goat polyclonal anti-NPRC	Sigma-Aldrich	SAB2501867
Rabbit polyclonal anti-p-p38MAPK	Cell Signaling Technology	Cat# 9211; RRID:AB_331641
Rabbit polyclonal anti-P38MAPK	Cell Signaling Technology	Cat# 9212; RRID:AB_330713
Rabbit polyclonal anti-pS660 HSL	Cell Signaling Technology	Cat#4126; RRID:AB_490997
Rabbit polyclonal anti-pS563 HSL	Cell Signaling Technology	Cat#4139; RRID:AB_2135495
Rabbit polyclonal anti-HSL	Cell Signaling Technology	Cat# 4107; RRID:AB_2296900
Rabbit monoclonal anti-GAPDH	Cell Signaling Technology	Cat# 2118; RRID:AB_561053
DAPI	Sigma-Aldrich	Cat#D9542
Lectin-rhodamine	Vector Laboratories	Cat#B-1105; RRID:AB_2336489
Biological Samples		
Brown adipocytes from humans	N/A	Broeders et al., 2015
White adipocytes from humans	N/A	Broeders et al., 2015
scWAT biopsies from humans	N/A	Barquissau et al., 2018
Plasma samples from humans	N/A	Vosselman et al., 2015
Chemicals, Peptides, and Recombinant Proteins		
Albumin	Sigma-Aldrich	Cat#A7030
Isoproterenol	Sigma-Aldrich	Cat#I5627
Atrial Natriuretic Peptide human	Sigma-Aldrich	Cat#A1663
Ripa buffer	Sigma-Aldrich	Cat#R0278
Protease inhibitor cocktail	Sigma-Aldrich	Cat# P8340/P5726/P0044
Collagenase	Sigma-Aldrich	Cat#C-6885
Qiazol	QIAGEN	Cat#79306
Fast SYBR green Master Mix	Life technology	Cat#4385614
Taqman Fast Master Mix	Life technology	Cat#4444558
Rnase inhibitor	Applied Biosystem	Cat# N8080119
Critical Commercial Assays		
Mouse Brain Natriuretic Peptide ELISA Kit	Cusabio	CSB-E07971m
Mouse Atrial Natriuretic Peptide ELISA kit	Cusabio	CSB-E04848m
Human Brain Natriuretic Peptide ELISA Kit	Cusabio	CSB-E07970h
Human Pro Atrial Natriuretic Peptide ELISA kit	Cusabio	CSB-E05149h
Free Glycerol reagent	Sigma	Cat#F6428
NEFA C kit	Wako	Cat#91898/91696
QIAGEN RNeasy kit	QIAGEN	Cat #74106
Kit High capacity cDNA Reverse Transcription kit	Applied Biosystem	Cat#4368814
BCA pierce kit	ThermoScientific	Cat # 23225
[18F]fluorodeoxyglucose (^{18}F-FDG) GlucoTep®	Cyclopharma	Cat # FDGTCPRECH
Vetflurane	Virbac	Cat # 200265

(*Continued on next page*)

Continued

REAGENT or RESOURCE	SOURCE	IDENTIFIER
Experimental Models: Organisms/Strains		
Mouse: B6.129P2-*Nppa*^{tm1Unc}/J	The Jackson Laboratory	https://www.jax.org/strain/002685
Mouse: C57BL6/J	Janvier Laboratories	https://www.janvier-labs.com/
Oligonucleotides		
See Tables S1 and S2	N/A	N/A
Software and Algorithms		
GraphPad	GraphPad software	https://www.graphpad.com/
ImageLab 4.2 version software	Biorad	http://www.bio-rad.com/
ImageJ	NIH	https://imagej.nih.gov/ij/
R software	N/A	https://www.R-project.org/
Corrplot Version 0.84	N/A	Wei and Simko, 2017
Nucline	Mediso	http://www.mediso.com
VivoQuant	InviCRO	https://invicro.com/vivoquant-home/
Other		
Rectal thermometer EcoScan Temp4/5/	Eutech Instruments	http://www.eutechinst.com
NanoScan TEP/CT	Mediso	http://www.mediso.com
Vivid7 echograph	GE Healthcare	N/A
14 MHz transducer i13L	GE Healthcare	N/A

RESOURCE AVAILABILITY

Lead Contact

Further information and requests for resources and reagents should be directed to and will be fulfilled by the Lead Contact, Cedric Moro (cedric.moro@inserm.fr).

Materials Availability

This study did not generate new unique reagents.

Data and Code Availability

This study did not generate/analyze new datasets.

EXPERIMENTAL MODEL AND SUBJECT DETAILS

Clinical studies and human subjects

Study 1

Ancillary study of the DiOGenes (Diet, Obesity and Genes) European Framework project (NCT00390637). For a thorough description of the overall objective and goals of this multicenter, randomized, controlled dietary intervention study, see Larsen et al. (2010). Briefly, the study examined the effects of dietary macronutrients on weight regain and cardiovascular risk factors. Inclusion and exclusion criteria for study participation were previously outlined (Larsen et al., 2010). The DiOGenes study included 938 participants aged 27-63 years from eight European countries; however, the present study used only a subgroup of 79 men and women who had high or medium *UCP1* gene expression in subcutaneous white adipose tissue as previously described (Barquissau et al., 2018) and *GCA* expression data available. Only baseline data were used in the present investigation.

Study 2

To investigate the effect of acute cold on circulating NP levels, each subject underwent a mild cold experiment. This experiment started with one-hour baseline measurements during thermoneutral conditions. Subsequently, subjects were exposed to one hour of mild cold exposure, in which a standardized cooling protocol was used. The mild cold experiment was conducted in a specially equipped air-permeable tent (Colorado altitude training, USA), in which ambient temperature could be tightly controlled. During baseline and the mild cold period, subjects wore standardized clothing (shorts and a t-shirt; 0.19 clo). Energy expenditure was continuously measured while body temperatures, skin perfusion (vasoconstriction) and heart rate were sampled each minute. Blood pressure was measured each 15 minutes as well as thermal comfort and thermal sensation via Visual Analog Scales (VAS).

These data have been reported previously (Vosselman et al., 2015). Muscle shivering was monitored by means of EMG and VAS scales. Venous blood samples were taken during baseline and one hour after the onset of cold exposure.

Mice

Eight weeks old *Nppa*−/− male mice (B6.129P2-*Nppa*^{tm1Unc}/J mice were backcrossed to C57BL/6J mice for at least ten generations) and their littermate control *Nppa*+/+ were used. Mice were fed with a normal chow diet (Ssniff) and were housed in a pathogen-free barrier facility (12h light/dark cycle) with *ad libitum* access to water and food in standard animal care facility rooms at 21°C (RT). For cold exposure experiments, at 7 a.m. animals were placed singly and exposed for 5 hours at 4°C with water access but without food. For acclimation to thermoneutrality, mice were transferred to a chamber with controlled ambient temperature at 30°C for four consecutive weeks. Rectal temperature was monitored using an EcoScan Temp4/5/ thermometer (Eutech Instruments) each hour during cold exposure or at indicated time points.

At the end of the protocol, mice were decapitated and blood was collected into EDTA tubes containing protease inhibitors. Organs and tissues were rapidly excised and either snap frozen in liquid nitrogen before being stored at −80°C or processed for histology. All experimental procedures were approved by our institutional animal care and use committee CEEA122 (protocol# 2016122311033178) and performed according to INSERM guidelines for the care and use of laboratory animals.

Human primary adipocytes culture

Adipocytes derived from human BAT and WAT were obtained and differentiated as described previously (Broeders et al., 2015; Nascimento et al., 2018; Wu et al., 2012). The study was reviewed and approved by the ethics committee of Maastricht University Medical Center (METC 10-3-012, NL31367.068.10, NCT03111719). Informed consent was obtained before surgery. In brief, the stromal vascular fraction was obtained from prevertebral BAT and subcutaneous WAT from the same area during thyroid surgery using a collagenase digestion. Differentiation was initiated for 7 days with differentiation medium containing biotin (33 μM), pantothenate (17 μM), insulin (100 nM), dexamethasone (100 nM), IBMX (250 μM), rosiglitazone (5 μM), T3 (2 nM), and transferrin (10 μg/ml). Cells were transferred to maintenance medium consisting of biotin (33 μM), pantothenate (17 μM), insulin (100 nM), dexamethasone (10 nM), T3 (2 nM), and transferrin (10 μg/ml) for another 5 days.

Mouse primary adipocytes culture

SVF from iWAT was obtained from 6-week-old WT mice as previously described (Planat-Benard et al., 2004). iWAT was dissected, mechanically dissociated and digested for 30min at 37°C with collagenase (collagenase NB 4 Standart Grade from Coger, concentration of 0.4 U/ml diluted in proliferative medium (αMEM plus 0.25 U/ml amphotericin, 100 U/ml penicillin, 100 mg/ml streptomycin, 0.016 mM biotin, 100 μM ascorbic acid, 0.018 mM pantothenic acid and 10% new-born calf serum). After filtration, red blood cells lysis and centrifugation, the pellet was resuspended in proliferative medium. SVF cells were then counted, plated at 10000 cells/cm^2 and rinsed in PBS 3 hours after plating. Cells were maintained at 37°C (5% CO_2) and re-fed every 48h. Adherent cells were grown to 80% confluency in proliferative medium. Cells were then exposed to an adipogenic cocktail (proliferative medium supplemented with 5 μg/ml insulin, 2 ng/ml T3, 33.3 nM dexamethazone, 10 μg/ml transferrin and 1 μM rosiglitazone) and used after 8 days of differentiation.

METHOD DETAILS

Blood analyses

Human and mouse plasma ANP and BNP were measured with Human Atrial Natriuretic Peptide ELISA kit (Cusabio) and Mouse Atrial Natriuretic Peptide ELISA kit (Cusabio), Human Brain Natriuretic Peptide ELISA kit (Cusabio), and Mouse Brain Natriuretic Peptide ELISA kit (Cusabio), respectively following manufactory instructions. Glycerol was measured by enzymatic assay (Free Glycerol reagent, Sigma), NEFA and TG were measured using the NEFA C kit (Wako) and TG reagent (sigma). Glucose and ketone bodies levels were measured using a glucometer (Accucheck; Roche, Meylan, France) and blood β-ketone bodies meter (Freestyle Optium H meter, Abbot) respectively. Plasma insulin was measured using an ultrasensitive ELISA kit (ALPCO Diagnostics, Salem, New Hampshire).

Echocardiography

Echocardiography was carried out with a Vivid7 echograph (GE Healthcare) and a 14 MHz transducer (i13L, GE) on lightly anesthetized (1% isoflurane in air) mice placed on a heating pad. Left ventricular walls and cavity dimensions were obtained from parasternal short axis view at mid-ventricular level during Time Movement mode acquisition. LV mass was estimated by a spherical approximation. LV ejection fraction was measured from parasternal long axis view by delineating LV chamber area in diastole and systole. The operator was blind from mice genotype.

^{18}F-FDG PET/CT

Positron emission tomography-computed tomography imaging with [^{18}F]fluorodeoxyglucose (^{18}F-FDG PET/CT) was performed as previously described (Wang et al., 2012). Briefly, mice were placed singly in cages, with water but without food and bedding, for 4h

fasting either at 4°C or RT before transfer to the imaging lab. Then mice were injected intraperitoneally with 10 to 14.5 MBq of ^{18}F-FDG (GlucoTep® Cyclopharma, S^{t}-Beauzire, France) and placed back into their respective cage either kept on ice or remaining on a heating pad (RT) for 1h. After anesthesia with 4% isoflurane, mice were placed in 36°C imaging chambers for a 15 min PET acquisition (NanoScan PET/CT *Mediso Ltd, Hungary*) 1h post ^{18}F-FDG injection and for a 6 min CT scan imaging (720 projections, semi-circular scan method, X-ray energy: 35kVp, exposure time: 450ms, voxel size: 251 × 251 × 251μm). PET acquisitions were performed in list-mode and reconstructed with a three-dimensional iterative algorithm (Tera-Tomo 3D, full detector model and low regularization; *Mediso Ltd, Hungary*) with four iterations and six subsets and a voxel size of 0.4 × 0.4 × 0.4 mm. All images were automatically corrected for radioactive decay during acquisition by the manufacturer software setting (Nucline, *Mediso Ltd, Hungary*). CT images were automatically fused to PET images and were also used for attenuation correction of PET images during their reconstruction. After acquisition, mice were placed back in clean cages with free access to food and water at RT. Processing of reconstructed images has been performed with VivoQuant software (InviCRO). 3D volumes of interest (VOIs) were drawn manually on the CT (part of left quadriceps) giving access to muscle mean ^{18}F-FDG uptake (kBq.g^{-1}) or, for BAT, by semi-automatic segmentation based on connected pixels threshold to calculate BAT ^{18}F-FDG uptake (kBq) and metabolic volume (mm^3).

Cellular cooling

Fully differentiated inguinal mouse primary adipocytes were kept in a 37°C incubator with 5% CO_2 before experiments. Before cooling treatment, medium was refreshed with prewarmed adipogenic cocktail. For cooling, culture plates were taken out from the home incubator (37°C) and immediately transferred to another incubator set at 31°C for 5 hours.

Adipocyte lipolysis

Fresh eWAT pads were dissected from mice and put into phosphate-buffered saline (PBS) at 37°C. Adipose tissue depots were cut into small pieces and transferred into Krebs-Ringer bicarbonate buffer (pH 7.4) containing 0.5 mM CaCl2, 238 mg/100ml HEPES, 108 mg/100 mL glucose, 3.5% BSA, and 1 mg/ml collagenase (C-6885, Sigma) at 37°C for 20 min. At the end of digestion, the fat cell suspension was filtered and rinsed three-times. Isolated packed adipocytes were diluted to 1/10th and incubated in Krebs-Ringer bicarbonate for basal lipolysis determination and 1μM isoproterenol or 1μM ANP for lipolysis determination. Incubations were carried out for 90 min at 37°C and then placed on ice to stop lipolysis. Glycerol was measured by enzymatic assay (Free Glycerol reagent, Sigma,) and NEFA were measured using the NEFA C kit (Wako).

Histology

Adipose tissues and livers were fixed with 4% paraformaldehyde in PBS, dehydrated, embedded in paraffin, and cut into 7μm sections. Sections were stained with hematoxylin and eosin using standard protocols. For Oil Red O (ORO) staining, livers were fixed in 4% paraformaldehyde in PBS, cryoprotected in 30% sucrose at 4°C and cut into 7μm sections using cryostat. ORO staining was performed as standard procedures.

Immunofluorescence

iBAT sections (300 μm) were incubated in blocking solution (2% normal horse serum and 0.2% Triton X-100 in PBS) for 4 hours at room temperature (RT) and then incubated with the lipid probe BODIPY 558/568 C12 (1:1000) before nuclei being stained with DAPI (Sigma Aldrich). iBAT sections were also incubated with lectin-rhodamine (1/250, Vector Laboratories) overnight at 4°C and nuclei stained with DAPI. Imaging was performed using a confocal Laser Scanning microscope (LSM 780, Carl Zeiss) and image analysis was performed using Fiji software (NIH).

Hepatic glycogen content

Liver samples were weighed and homogenized in acetate buffer (0,2M, pH 4.8). After centrifuging the samples at 12 000 g for 10min, supernatant was transferred into clean tubes and divided in two aliquots. An aliquot of each homogenate was mixed with amyloglucosidase (Sigma) and incubated at 55°C for 15 minutes. The other one was mixed with water and incubated at 4°C for 15 minutes. Glucose content was measured as previously described below. Samples were analyzed in duplicate and the results determined as μg glycogen per mg tissue.

Hepatic triglycerides content

Liver triglycerides were extracted using Folch extraction procedure, as previously described (Monteillet et al., 2018). This procedure consist in the addition of a chloroform/methanol 2/1 solution to 100 mg of frozen liver (1.7mL for 100mg of tissue), and then a crushing with Fast Prep®. The solution was centrifuged twice (2,000 g; 10 min; 4°C), and 2mL of NaCl was added to the supernatant previously removed. Two phases were created, and the inferior organic phase that contains triglycerides was kept. After chloroform evaporation, triglycerides were diluted in 100μL of propanol and measured with a colorimetric kit (DiaSys, Holzheim, Germany).

Mitochondrial respiration

Freshly isolated tissues were carefully minced and homogenized in homogenization buffer (sucrose 250mM, Trizma-HCl 120mM, EGTA 1mM, 0.3% free fatty acid BSA, pH 7.2) and filtered (100μm) at 4°C. The homogenates (20μl and 100μl of BAT and WAT

homogenate respectively) were placed into a magnetically stirred oxygen electrode chamber set to 37°C (OROBOROS Oxygraph-2k, OROBOROS Instruments Corp, Innsbruck, Austria) in respiration buffer (KCl 125mM, Trizma-HCl 120mM, EGTA 1mM, KH2PO4 10mM, 0.1% free fatty acid BSA, pH 7.2) in the presence of substrates (Glutamate 10mM, Malate 2mM, Succinate 10mM, Pyruvate 5.45mM, ADP 3.4mM and MgCl2 2mM). The chamber was closed, and the homogenates were incubated to determine the basal respiratory rate. Antimycin (2.3μM) was added to measure basal mitochondrial-derived oxygen consumption. Oxygen consumption rate was determined from the slope of a plot of O2 concentration versus time and adjusted to protein content of the homogenate.

SeaHorse

For oxygen consumption measurements, differentiated adipocytes were incubated for 1 h at 37 C in unbuffered XF assay medium supplemented with 2 mM GlutaMAX, 1 mM sodium pyruvate, and 25 mM glucose. To determine mitochondrial uncoupling, oxygen consumption was measured using bio-analyzer from Seahorse Bioscience after addition of 2 μM oligomycin, which inhibited ATPase, followed by indicated concentrations of ANP or 1 μM NE. Maximal respiration was determined following 0.3 μM FCCP. 1 mM antimycin A and rotenone was added to correct for non-mitochondrial respiration (Broeders et al., 2015).

Real-time qPCR

Total RNA from tissue was isolated using QIAGEN RNeasy kit (QIAGEN, GmbH Hilden, Germany) following manufacturer's protocol. The quantity of the RNA was determined on a Nanodrop ND-1000 (Thermo Scientific, Rockford, IL, USA). Reverse-transcriptase PCR was performed using the Multiscribe Reverse Transcriptase method (Applied Biosystems, Foster City, CA). Quantitative Real-time PCR (qRT-PCR) was performed in duplicate using the ViiA 7 Real-time PCR system (Applied biosystems). All expression data were normalized by the $2^{(-\Delta Ct)}$ method using, *18S* in mice and *PUM1* and *GUSB* in human cultures, as internal control. Correlation with thermogenic markers gene expression was assessed using the Biomark HD system with 96.96 Dynamic Array IFC (Fluidigm) and TaqMan assays (Applied Biosystems) as described in Barquissau et al. (2018). Data were normalized using the $2^{-\Delta Ct}$ method and *PUM1* as reference gene. The primers used are listed in the Tables S1 and S2.

Western blot

Proteins were extracted from tissues using Ripa buffer and protease inhibitor cocktail (Sigma-Aldrich). Tissues homogenates were centrifuged twice for 20 min at 12700 rpm and supernatants were quantified with BCA pierce kit (ThermoScientific). Equal amount of proteins were run on a 4%–20% SDS-polyacrylamide gel electrophoresis (Biorad), transferred onto nitrocellulose membrane (Bio-Rad) and incubated overnight at 4°C with primary antibodies, Rabbit anti-Actin (1:10000, CST, #4970), Rabbit anti-ATGL (1:1000, CST #2138s), Rabbit anti-GAPDH (1:1000, CST, #2118), Mouse anti-GLUT1 (1:1000, Abcan, ab40084), Rabbit anti-G6PC (Rajas et al., 2007) (1:2000), Rabbit anti-pS660 HSL (1:1000, CST, #4126), Rabbit anti-pS563 HSL (1:1000, CST, #4139s), Rabbit anti-HSL (1:1000, CST, #4107), Rabbit anti-NPRA (1:1000, Abcam, ab154266), Goat anti-NPRC (1:1000, Sigma, SAB2501867), Rabbit anti-PEPCK (1:7000, Santa cruz, #32879), Rabbit anti-p-p38MAPK (1:1000, CST, #9211), Rabbit anti-P38MAPK (1:1000, CST, #9212), Rabbit anti-UCP1 (1:1000, Abcam, ab10983). Subsequently, immuno-reactive proteins were blotted with anti-rabbit or goat horseradish peroxidase-labeled secondary antibodies for 1h at room temperature and revealed by enhanced chemiluminescence reagent (SuperSignal West Femto, Thermo Scientific), visualized using ChemiDoc MP Imaging System and data analyzed using the ImageLab 4.2 version software (Bio-Rad Laboratories, Hercules, USA).

QUANTIFICATION AND STATISTICAL ANALYSIS

All statistical analyses were performed using GraphPad Prism 7.0 for Windows (GraphPad Software Inc., San Diego, CA), except for Figure 4A that was produced using the package corrplot of the R software (Wei and Simko, 2017). Normal distribution and homogeneity of variance of the data were tested using Shapiro-Wilk and F tests, respectively. Student's t tests, Mann-Whitney test or one-way ANOVA were performed to determine differences between groups/treatments. Two-way ANOVA followed by Bonferonni's post hoc tests were applied when appropriate. Univariate linear regressions were performed on parametric data. The false discovery rate for multiple testing was controlled by the Benjamini-Hochberg procedure with $p_{adj.}$ values ≤ 0.05 as threshold. All values in Figures are presented as mean ± SEM. Statistical significance was set at $p < 0.05$.

Cell Reports, Volume *32*

Supplemental Information

Atrial Natriuretic Peptide Orchestrates a Coordinated Physiological Response to Fuel Non-shivering Thermogenesis

Deborah Carper, Marine Coué, Emmani B.M. Nascimento, Valentin Barquissau, Damien Lagarde, Carine Pestourie, Claire Laurens, Justine Vily Petit, Maud Soty, Laurent Monbrun, Marie-Adeline Marques, Yannick Jeanson, Yannis Sainte-Marie, Aline Mairal, Sébastien Déjean, Geneviève Tavernier, Nathalie Viguerie, Virginie Bourlier, Frank Lezoualc'h, Audrey Carrière, Wim H.M. Saris, Arne Astrup, Louis Casteilla, Gilles Mithieux, Wouter van Marken Lichtenbelt, Dominique Langin, Patrick Schrauwen, and Cedric Moro

Supplemental Information

Atrial natriuretic peptide orchestrates a coordinated physiological response to fuel non shivering thermogenesis

Deborah Carper, Marine Coue, Emmani Nascimento, Valentin Barquissau, Damien Lagarde, Carine Pestourie, Claire Laurens, Justine Vily Petit, Maud Soty, Laurent Monbrun, Marie-Adeline Marques, Yannick Jeanson, Yannis Sainte-Marie, Aline Mairal, Sébastien Dejean, Geneviève Tavernier, Nathalie Viguerie, Virginie Bourlier, Frank Lezoualc'h, Audrey Carrière, Wim H.M. Saris, Arne Astrup, Louis Casteilla, Gilles Mithieux, Wouter van Marken Lichtenbelt, Dominique Langin, Patrick Schrauwen and Cedric Moro

SUPPLEMENTAL FIGURES

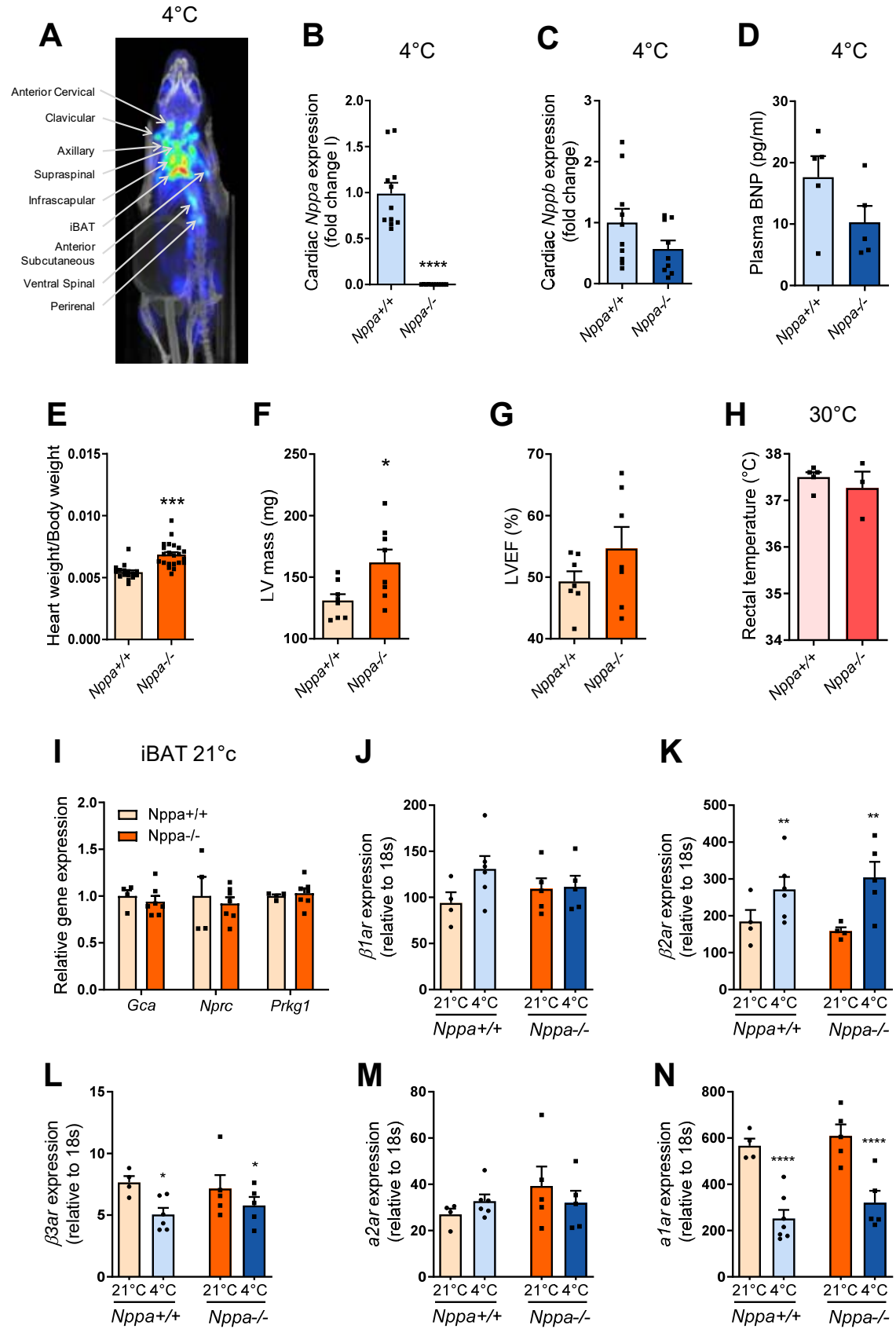

Figure S1. ANP is essential for non-shivering thermogenesis during acute cold exposure. Related to Figure

1

(A) Representative ^{18}F-FDG PET/CT images of BAT recruitment around the neck in mice exposed for 5h to 4°C
(B-C) Cardiac *Nppa* expression (B) and cardiac *Nppb* expression (C) in *Nppa*+/+ and *Nppa*-/- mice (n=11)
(D) Plasma BNP in *Nppa*+/+ and *Nppa*-/- mice after acute cold exposure (n=5-6)
(E) Heart weight to body weight ratio from *Nppa*+/+ and *Nppa*-/- mice (n=16-22)
(F) Left ventricular (LV) mass from *Nppa*+/+ and *Nppa*-/- mice (n=8)
(G) Left ventricular ejection fraction (LVEF) from *Nppa*+/+ and *Nppa*-/- mice (n=7)
(H) Rectal temperature of *Nppa*+/+ and *Nppa*-/- mice housed at thermoneutrality (30°C) (n=3-5)
(I) Relative mRNA levels of *Gca, Nprc* and *Prkg1* in iBAT from *Nppa*+/+ and *Nppa*-/- mice housed at 21°C (n=4-7)
(J-K-L-M-N) Relative mRNA levels of *β1ar* (J), *β2ar* (K), *β3ar* (L), *α2ar* (M) and *α1ar* (N) in iBAT from *Nppa*+/+ and *Nppa*-/- mice housed at 21°C or after acute cold exposure (n=4-6)
Results are shown as mean ± SEM. *p<0.05, **p<0.01, ***p<0.001, ****p<0.0001

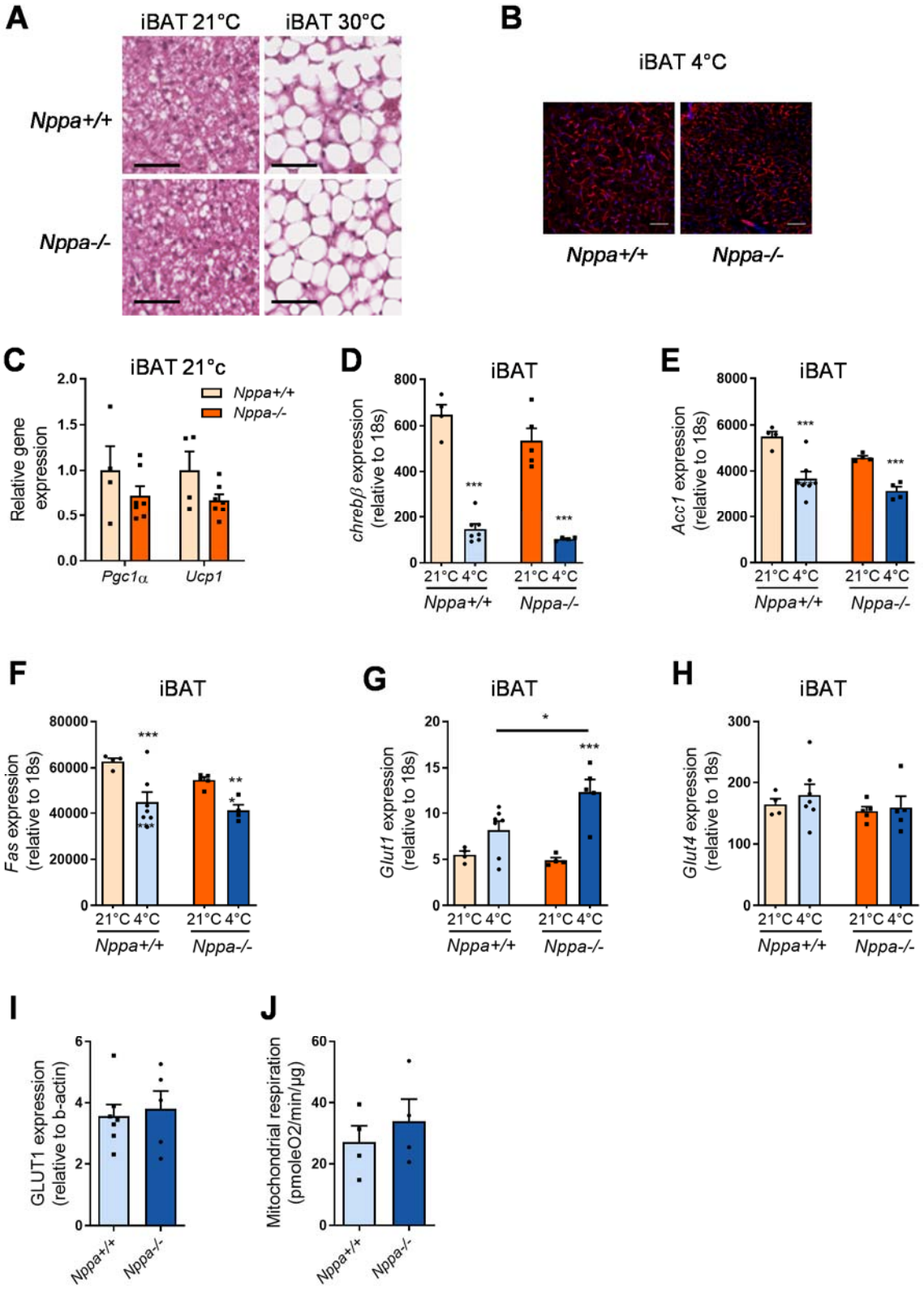

Figure S2. ANP-deficiency induces BAT morphological and molecular changes. Related to Figure 2
(A) Representative Hematoxylin/Eosin staining of iBAT from *Nppa*+/+and *Nppa*-/- mice housed at 21°C or 30°C. Scale bar = 50µm
(B) Representative Lectin/DAPI staining of iBAT from *Nppa*+/+and *Nppa*-/- mice after cold exposure. Scale bar = 50µm
(C) Relative mRNA levels of *Pgc1α* and *Ucp1* in iBAT from *Nppa*+/+ and *Nppa*-/- mice housed at 21°C (n=4-7)
(D-E-F-G-H) Relative mRNA levels of *Chrebpβ* (D), *Acc1* (E), *Fas* (F), *Glut1* (G) and *Glut4* (H) in iBAT

from *Nppa*+/+ and *Nppa*-/- mice housed at 21°C of after cold exposure (n=4-7)
(I) Relative GLUT1 protein level in iBAT of *Nppa*+/+ and *Nppa*-/- mice after cold exposure (n=5-7)
(J) Mitochondrial respiration of BAT homogenates from *Nppa*+/+ and *Nppa*-/- mice after cold exposure (n=4)
Results are shown as mean ± SEM. *p<0.05, **p<0.01, ***p<0.001

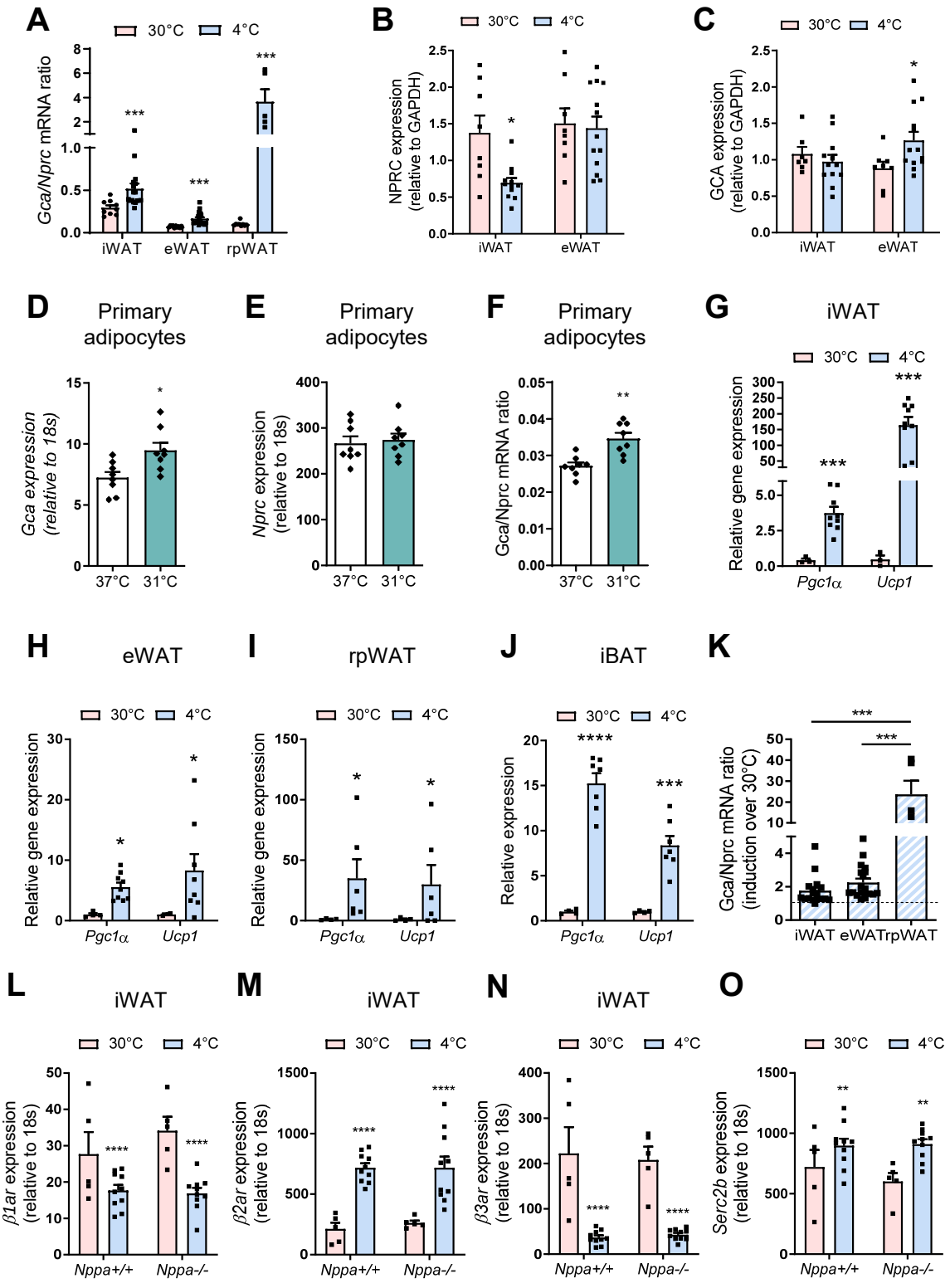

Figure S3. ANP is required for beige adipocyte recruitment during acute cold exposure. Related to Figure 3

(A) *Gca/Nprc* mRNA ratio in iWAT, eWAT and rpWAT of WT mice housed at 30°C (n=9-10) and after acute cold exposure (5h at 4°C) (n=4-19)

(B-C) Relative NPRC (B) and GCA (C) protein level in iWAT and eWAT of WT mice housed at 30°C (n=8) and after acute cold exposure (4°C) (n=13).

(D-E-F) Relative mRNA levels of *Gca* (D) and *Nprc* (E) and *Gca/Nprc* mRNA ratio (F) in mouse primary adipocytes cultured at 37°C or after incubation at 31°C (n=8)

(G-H-I-J) Relative mRNA levels of *Pgc1α* and *Ucp1* in iWAT (G), eWAT (H), rpWAT (I) and iBAT (J) of WT mice at 30°C and after acute cold exposure (5h at 4°C) (n=4-8)
(K) *Gca/Nprc* mRNA induction in iWAT (n=17), eWAT (n=19) and rpWAT (n=5) of WT mice after acute cold exposure
(L-M-N-O) Relative mRNA levels of *β1ar* (L), *β2ar* (M), *β3ar* (N), *Serca2b* (O) in iWAT from *Nppa*+/+ and *Nppa*-/- mice housed at 30°C or after acute cold exposure (n=5-10) Results are shown as mean ± SEM. *p<0.05, **p<0.01, ***p<0.001, ****p<0.0001

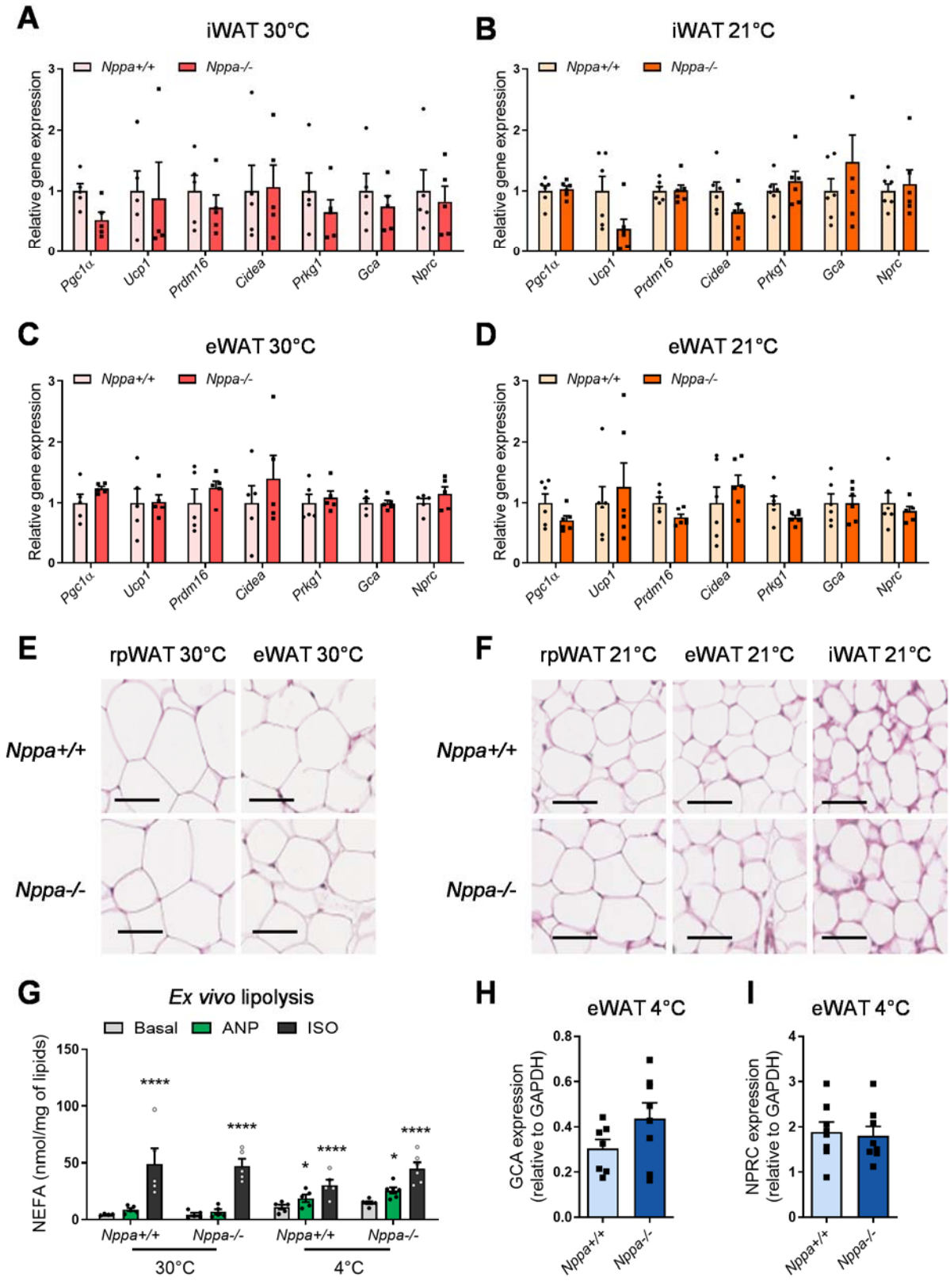

Figure S4. ANP is required for white adipocyte lipolysis during acute cold exposure. Related to Figure 3

(A-B) Relative mRNA levels of thermogenic and NP-signaling genes in iWAT from *Nppa*+/+and *Nppa*-/- mice housed at 30°C (n=5) (A) and room temperature (21°C) (n=6) (B)

(C-D) Relative mRNA levels of thermogenic and NP-signaling genes in eWAT from *Nppa*+/+ and *Nppa*-/- mice housed at 30°C (n=5) (C) and RT (n=6) (D)

(E) Representative Hematoxylin/Eosin staining of rpWAT and eWAT from *Nppa*+/+ and *Nppa*-/- mice housed at 30°C. Scale bar = 50µm
(F) Representative Hematoxylin/Eosin staining of rpWAT, eWAT and iWAT from *Nppa*+/+ and *Nppa*-/- mice housed at room temperature (21°C). Scale bar = 50µm
(G) *Ex vivo* adipocyte lipolysis in eWAT under basal, ANP and isoproterenol-stimulated conditions from *Nppa*+/+ and *Nppa*-/- mice housed at 30°C and after acute cold exposure (n=5-8)
(H) Relative GCA protein level in eWAT of *Nppa*+/+ and *Nppa*-/- mice after acute cold exposure (n=8)
(I) Relative NPRC protein level in eWAT of *Nppa*+/+ and *Nppa*-/- mice after acute cold exposure (n=8)
Results are shown as mean ± SEM. *$p<0.05$

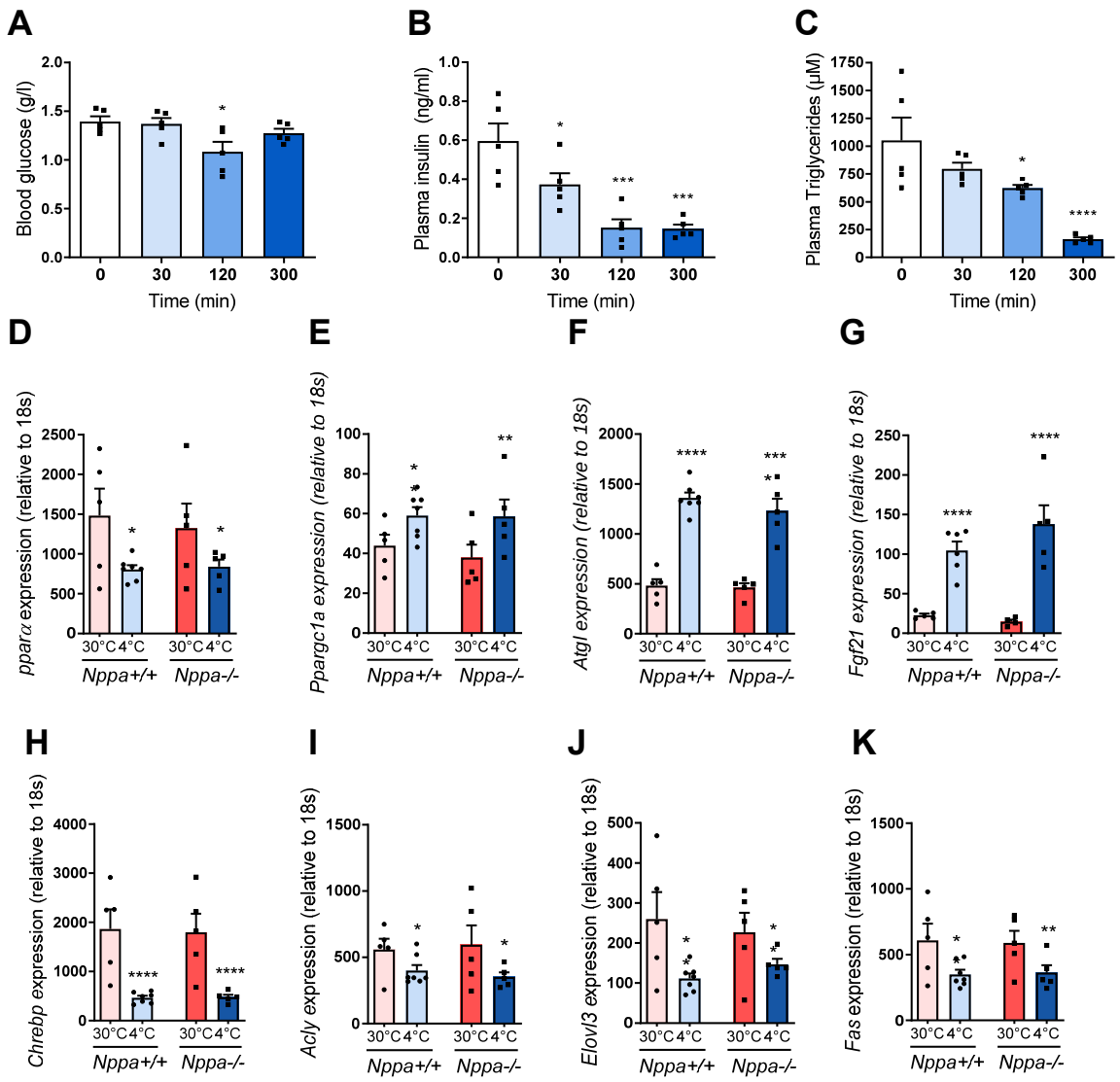

Figure S5. ANP deficiency impairs plasma triglycerides and glucose responses to cold. Related to Figure 4
(A-B-C) Blood glucose (A), plasma insulin (B) and plasma triglycerides (C) levels during acute cold exposure in WT mice (n=5)
(D-E-F-G-H-I-J-K) Relative mRNA levels of *Pparα* (D), *Pgc1α* (E), *Atgl* (F), *Fgf21* (G), *Chrebp* (H), *Acly* (I), *Elovl3* (J), and *Fas (K)* in liver of *Nppa*+/+ and *Nppa*-/- mice at 30°C and after acute cold exposure (n=5-7)
Results are shown as mean ± SEM. *p<0.05, **p<0.01, ***p<0.001, ****p<0.0001

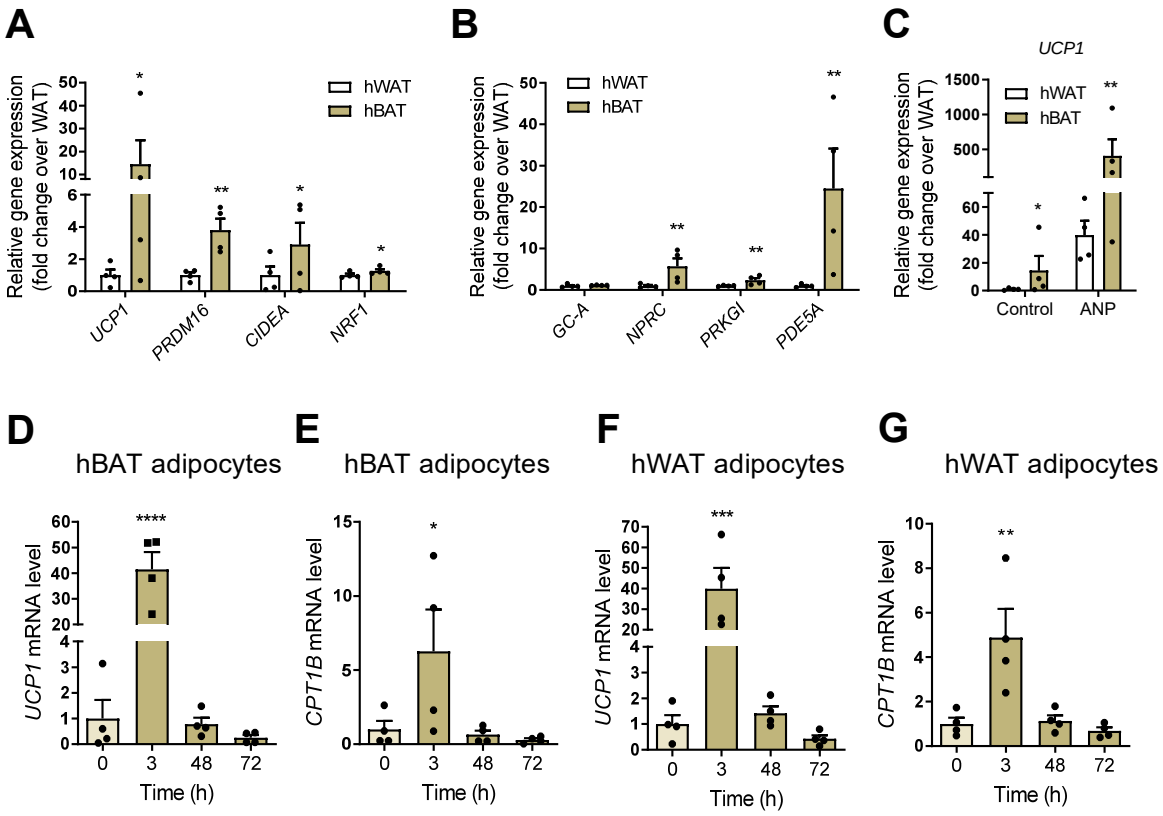

Figure S6. ANP activates mitochondrial uncoupling in BAT and a thermogenic program in human primary brown/beige and white adipocyte. Related to Figure 6

(A) Relative mRNA levels of *UCP1*, *PRDM16, CIDEA* and *NRF1* in human primary white adipocytes (hWAT) and human primary brown/beige adipocytes (hBAT) (n=4)

(B) Relative mRNA levels of *GC-A*, *NPRC*, *PRKG1* and *PDE5A* in hWAT and hBAT (n=4)

(C) Relative mRNA levels of *UCP1* in hWAT and hBAT in absence (control) or presence of ANP 100 nM (n=4)

(D-E) Relative mRNA levels of *UCP1* (D) and *CPT1B* (E) in hBAT treated with ANP for 3, or 72h (n=4)

(F-G) Relative mRNA levels of *UCP1* (F) and *CPT1B* (G) in hWAT treated with ANP for 3, or 72h (n=4)

Results are shown as mean ± SEM. *p<0.05, **p<0.01, ***p<0.001, ****p<0.0001

SUPPLEMENTAL TABLES

Supplemental Table 1. List of primer and probe sequences used for real-time qPCR with Taqman chemistry. Related to Figures 1-6 and Figures S-6.

Gene symbol	Taqman Probe
Cidea	Mm00432554_m1
Cpt1b	Mm00487200_m1
Elovl3	Mm00468164_m1
Npr1	Mm00435324_m1
Npr3	Mm00435329_m1
Pck1	Mm00440636_m1
Pgc1α	Mm01208835_m1
Plin2	Mm00475794_m1
Prkg1	Mm00440954_m1
Ucp1	Mm01244861_m1
18S	Hs99999901_s1
CA4	Hs00426343_m1
CIDEA	Hs00154455_m1
CITED1	Hs00918445_g1
CPT1B	Hs00972284_m1
CYC1	Hs00357717_m1
DIO2	Hs00988260_m1
ELOVL3	Hs00537016_m1
GUSB	Hs99999908_m1
NDUFB6	Hs00159583_m1
NRF1	Hs00602161_m1
PLIN5	Hs00965990_m1
PPARa	Hs00231882_m1
PRDM16	Hs00223161_m1
PUM1	Hs00472881_m1
SIRT3	Hs00202030_m1
TFAM	Hs01082775_m1
UCP1	Hs00222453_m1

Supplemental Table 2. List of primer and probe sequences used for real-time qPCR with Sybr chemistry. Related to Figures 1-4 and Figures S1-5.

Gene symbol	Forward	Reverse
A1ar	TGTGCCCGGAAATGTACTGG	TCTGTGGCCCAATGTTGATAAG
A2ar	AATTGCAGACGGTCCTCTCG	TGGCACCCTGCCTTTCATAG
Acc1	GCCTCTTCCTGACAAACGAG	TGACTGCCGAAACATCTCTG
Acly	ATGCCCCAAGATTCAGTCCC	ACGATGGCCTTGGTATGTCG
Atgl	TCCTTAGGAGGAATGGCCTAC	TCCTCTTCCTGGGGGACAAC
Cd36	CGCTGTGGAAATGGTGTGTT	GAAGGCAGCAACTTCTAGAACAG
Chrebp	TCTGCAGATCGCGTGGAG	CTTGTCCCGGCATAGCAAC
Cpt1a	TTGGAAGTCTCCCTCCTTCA	GCCCATGTTGTACAGCTTCC
Fas	TGGTGAATTGTCTCCGAAAAG	CACGTTCATCACGAGGTCATG
Fgf21	CGTCTGCCTCAGAAGGACTC	AAGGCTCTACCATGCTCAGG
G6p	ACACCGACTACTACAGCAACAG	CCTCGAAAGATAGCAAGAGTAG
Glut1	TCAACACGGCCTTCACTG	CACGATGCTCAGATAGGACATC
Glut4	ACTCTTGCCACACAGGCTCT	CCTTGCCCTGTCAGGTATGT
Lpl	TTATCCCAATGGAGGCACTTT	CACGTCTCCGAGTCCTCTCTC
Nppa	CTGCTTCGGGGGTAGGATTG	TTCGGTACCGGAAGCTGT
Nppb	GCTGCTTTGGGCACAAGATA	ACAACAACTTCAGTGCGTTACAG
Ppara	AGTTCACGCATGTGAAGGCTG	TGTTCCGGTTCTTCTTCTGAATC
Prdm16	CAGCACGGTGAAGCCATTC	GCGTGCATCCGCTTGTG
Serca2b	ACCTTTGCCGCTCATTTTCCAG	AGGCTGCACACACTCTTTACC
β1ar	CTCGTCCGTCGTCTCCTTCTAC	GTCGATCTTCTTTACCTGTTTTTGG
β2ar	TTGCAGTGGATCGCTATGTTG	TGACCACTCGGGCCTTATTCT
β3ar	CCTTCAACCCGGTCATCTAC	GAAGATGGGGATCAAGCAAGC